Functional significance of multiple transcripts from mouse Ntrk2 gene locus

We found that multiple sense and antisense transcripts are expressed from the 3′-flanking genomic segment of TrkB-TM/JM-T2 exon in *Ntrk2* gene locus as is summarized in Fig. 6. In the present study we could not fully determine whether those transcripts encode protein products or are parts of microRNAs. To investigate *Ntrk2* gene expression mechanism, it would be necessary to identify the full-length of these transcripts.

We have identified two novel transcripts including genomic sequences from region c that encode TrkB-TK(−) splicing variants. We have also demonstrated that ISH signals with the antisense probe for region c are massively distributed in the developing mouse nervous system. Notably, the region c is transcribed from the opposite chain and the ISH signals are equally strong compared to the staining by the antisense probe. It is possible that the antisense transcripts form RNA–RNA duplexes with the novel TrkB transcripts to inhibit translation and/or splicing them as found for the human *BDNF* gene locus (Pruunsild et al., 2007). Hence *bona fide* functional expression domains of the novel TrkB product may be restricted within the antisense product negative areas including the telencephalic mantle zones at E12.5 and ependymal cell layers at P7 (Fig. 4). We have further observed that expressed TrkB isoforms including the novel variant had diverse distribution in Neuro-2a cells. These results indicate that TrkB isoforms have individual functions in their various intracellular locations, elaborating the neural structures at the site of expression *in vivo* (Fig. 7).

Earlier studies have identified some other TrkB variants such as TrkB-T-Shc (Stoilov et al., 2002), a TrkB-TK(+) receptor variant with deletions in the extracellular domain (Ninkina et al., 1997; Strohmaier et al., 1996) and a TrkB-TK(−) with a unique cytoplasmic tail (Garner et al., 1996) in various species. It is further known that both TrkA and TrkC have alternative splicing variants (Barker et al., 1993; Coulier et al., 1990; Esteban et al., 2006; Martin-Zanca et al., 1990), suggesting a common feature of Trk receptor family to create a variety of isoforms for diversifying ligand-binding or signal transduction properties. Considering the evolutional traits (Benito-Gutierrez et al., 2006), our new information might serve as a basis for identifying those elements that balance multiple ways of splicing.

We have observed that BDNF is poorly expressed at E12.5. Are functions of TrkB totally independent of BDNF? The conflict may be explained by their alternative ligands (Reichardt, 2006), such as NT-3 in the trigerminal ganglia (Davies et al., 1995) or by intracellular trafficking and/or broad diffusion of these neurotrophins (Altar and DiStefano, 1998). TrkB could further function as co-receptors for some G-protein coupled receptors or cell adhesion molecules, which is very independent of neurotrophins (Wiese et al., 2007). Such tantalizing scenarios would be subjects for future studies.

In conclusion, our results clearly indicate that TrkB mRNA expressions are strictly regulated at the level of transcription, splicing and/or subcellular localizations. Complex transcriptional regulations of mouse *Ntrk2* gene locus as well as the combinatorial expression profiles and diverse protein functions of each TrkB isoform may support multiple effect of BDNF in the developing nervous system.

Experimental methods

Animals

Time pregnant ICR mice (embryonic 12.5-day-old (E12.5)), postnatal 7-day-old (P7) and 8-week-old (8W) mice were purchased from Clea JAPAN to collect embryos, tissues and RNA samples. The experimental protocol was approved by the Ethics review Committee for Animal Experimentation of National Institute of Neuroscience (NCNP).

In situ hybridization

Preparation of digoxigenin-UTP-labeled RNA probes and *in situ* hybridization (ISH) were performed as described previously with slight modifications (Inoue et al., 1998). PCR was performed to amplify probe fragments of TrkB isoform-specific regions from mouse brain cDNA or those of intron regions from BAC (#RP23-141B16) DNA, and the amplified fragments were cloned into pBluescript II vector (Stratagene, USA). Primers were designed as follows: TrkB extracellular domain (forward, 5′-CATGGATCCTGACCCACTCCCCACCTTG-3′, reverse, 5′-CATAAGCTTCGACTC-CAGGCCGGCCCATG-3′), T1 (forward, 5′-GATCCCACTGGATGGGTAGCTGA-GATAAAG-3′, reverse, 5′-TAATTCAGGTCCATACTCCTGGCCACACAG-3′), T2 (forward, 5′-CTCGCTCGAGGAGATGTGGCCGTCCGGACTCATGAC-3′, reverse, 5′-CATAAGTCGACCCTGCTTTCCAGTGAGCGCGGTTGT-3′), TK (forward, 5′-CGGGGATCCGGTATCACCAACAGCCAGCTCAAGCCG-3′, reverse, 5′-CCCAAGCTTCTCGGTGGGCGGGTTACCCTCTGCCATC-3′), Region a (forward, 5′-CAGACCAGACCTACTCGAGGAAGGCAGAG-3′, reverse, 5′-CACGG-GCATCACGTGACTGAGCAACTTCG-3′), Region b (forward, 5′-GCACAT-CATGCCTTGTGAGCAGA-3′, reverse, 5′-CTTTGCCTTCCTGTTCGAGCTGC-3′), Region c (forward, 5′-GATCAAGGCATAGACGAAAGTAC-3′, reverse, 5′-GTTGACTCTGCTCAGGTTGTGCCAG-3′), Region d (forward, 5′-GTACATG-CACAGAGTGTATATGAC-3′, reverse, 5′-TCCTCCCAGAAGAAGCAGCAAC-3′), Region e (forward, 5′-TGAAGGCAGAGGAGGCTTACGCTGTG-3′, reverse, 5′-CAAGGGGGAAATGCAGAGGCGAAGTC-3′), Region f (forward, 5′-GACAGACAGCATGCTGGAGAAG-3′, reverse, 5′-GTGAGACTGAGATA-GACTCCCG-3′), Region g (forward, 5′-AAAGGCAGTTTTCTCTCACAGC-3′, reverse, 5′-GCTCTGTTCTGGTTATCTACAC-3′), Region h (forward, 5′-CGCTCTTCTAATGTAGGAACTC-3′, reverse 5′-ACTTCTGCCATCTCTTAG-GACC-3′). The probe for BDNF is prepared from the part of the coding region (150–774 nucleotides from ATG initiation codon).

Whole E12.5 embryos and P7 mouse brains were fixed with 4% paraformaldehyde (PFA) in phosphate buffered saline (PBS). 8W mouse brains were fixed by transcardial perfusion with PBS followed by 4% PFA in PBS at 4 °C. The embryos and brains were immersed in the fixative overnight at 4 °C, followed by treatments of a graded series of sucrose solutions (5 10 15 20%) in PBS, embedded in Tissue-Tek optimal cutting temperature (OCT) compound (Sakura Finetek, Japan), and frozen on a block of dry-ice. For E12.5 embryos, 18 μm frontal or coronal sections were serially collected on slide glasses coated by Vectabond Reagent (Vector Laboratories, Burlingame, CA). We further collected 25 μm frontal sections for P7 brains and 14 μm frontal sections for adult brains. To obtain the high sensitive and stringent results, the steps of hybridization and post-hybridization wash were carried out at 65 °C to avoid nonspecific bindings and the detection periods of each antisense and sense probe were always equal by using the high sensitive detection reagent containing polyvinyl alcohol. For ISH experiment in Figs. 2 and 3, ISH was performed with sense probes for EC, T1, T2 and region a and b, and we confirmed that no signal was detected with these sense probes. Stained sections were photographed under bright field system of a Keyence microscope (Biorevo) or a Leica microscope (DM5000B) equipped with a Leica digital camera (FX300).

Cloning of novel TrkB splicing variants by RT-PCR

Total RNA was prepared from P7 mouse cerebral cortices, cerebella and livers using the protocol provided by the manufacturer of TRIzoL reagent (Invitrogen, California, USA) and purified with RNeasy Mini Kit (Qiagen, Germany). One microgram of total RNA was converted into cDNA by reverse transcription (RT) using ReverTra Ace (TOYOBO, Japan) with oligo $d(T)_{12-18}$ primers (Invitrogen). Novel splicing variants were screened by RT-PCR using the following primer pairs; F1, F2 or F3 with R1 for region e, F1, F2, or F3 with R2 for region d, and F1, F2, or F3 with R3 or R4 for region c, as was represented in Figs. 5 and 6. As a negative control, the

template without RT reaction was used and we confirmed that few PCR products were amplified (data not shown). The forward primer and reverse primer sequences were as follows; Forward primers; F1 (5′-GGTCTGCCGTCTGCACGTCTG-3′), F2 (5′-GGTGCATCCCATTCACTGTG-3′), F3 (5′-CTGCTCAAGTTGGCGAGAC-3′), Reverse primers; R1 (5′-CAAGGGGGAAATGCAGAGGCGAAGTC-3′), R2 (5′-TCCTCCCAGAAGAAGCAGCAAC-3′), R3 (5′-GACAACAAAGGATGGCAGCGTG-3′), R4 (5′-GTTGACTCTGCTCAGGTTGTGCCAG-3′). The full-length cDNA of novel TrkB splicing variants was amplified by PCR using KOD plus (TOYOBO, Japan) with Primer F and Primer R represented in Figs. 5 and 6. These RT-PCR products were cloned into pBluescript II vector (Stratagene, USA) and sequenced.

Nucleotide sequence accession numbers

Nucleotide sequence accession numbers assigned by the DDBJ databases are AB377224 for T3 alpha and AB377225 for T3 beta.

Construction of FLAG-tagged TrkB variant expression vectors

TrkB-TK/-T1 isoforms and rat TrkB-T2 cDNA were subcloned into pcDNA3.1(−) expression vector (Invitrogen, Carlsbad, CA) as described previously (Ohira et al., 2005). Regarding mouse TrkB-T2, the cDNA was amplified from mouse embryonic cDNA via PCR with Primer F and the reverse primer positioned at the 3′ flanking sequence of the putative stop codon (5′-GGTTTGCATGGCAACCCCAC-3′) and the PCR product was subcloned into pcDNA3.1(−). TrkB-T3 alpha and beta cDNAs in pBluescript II described above were cut by *Apa*I and *Eco*RI respectively and subcloned into pcDNA3.1(−). As described previously, FLAG tag was inserted into the putative signal peptide cleavage site, which will not interfere with the ability of BDNF binding and autophosphorylation of TrkB-TK(+) (Haapasalo et al., 1999; Kryl et al., 1999).

Cell culture and transfection

Neuro-2a mouse neuroblastoma cells were maintained in Dulbecco's modified Eagle's minimum essential medium supplemented with 10% fatal bovine serum, 100 U/ml penicillin and 100 μg/ml streptomycin in humidified atmosphere containing 5% CO_2 at 37 °C. The cells (1.0×10^5 cells/well) were plated on 12-well plates containing glass coverslips coated with polyethyleneimine (0.1%) the day prior to transfection. TrkB variant constructs (1 μg/well) were introduced into the cells by TransFectin reagent (Bio-Rad, Hercules, CA).

Western blot analysis

Cells were lysed by 0.5% Nonidet P-40 in PBS with protease inhibitors for 15 min at 4 °C. After the lysed cells were centrifuged at 10,000 ×g for 15 min at 4 °C, the supernatants were denaturated with SDS-sample buffer and boiled for 3 min. In the case of deglycosilation of TrkB isoforms, the lysates were incubated with 1 U of *N*-glycosidase F (Roche, Indianapolis, IN)) in deglycosilation buffer (0.5% NP-40, 0.1% SDS, 1% 2-mercaptoethanol and 10 mM EDTA in PBS) before denaturating. Samples were subjected to sodium dodecyl sulfate-polyacrylamide gel electrophoresis (10% gel), and the proteins were blotted onto the PVDF membrane (Millipore, Bedford, MA). The blotted membranes were blocked in 5% skimmed milk in PBS. The blots were then incubated with anti-FLAG polyclonal antibody (diluted at 1/500; Sigma, St. Louis, MO) or anti-TrkB polyclonal antibody (diluted at 1/500; Santa Cruz Biotechnology, Santa Cruz, CA) at 4 °C overnight, and washed for 30 min in Tris buffered saline containing 0.05% Tween 20. They were incubated with the secondary antibody conjugated with horseradish peroxidase and the proteins were visualized with Western Lightning enhanced chemiluminescence system (Perkin Elmer, Waltham, MA).

Immunocytochemistry

Cells were fixed for 15 min in PBS containing 4% PFA and permeabilized for 5 min in 0.05% Triton X-100 in PBS. After blocking with 4% goat serum in PBS for 2 h at RT, the cells were incubated overnight at 4 °C with anti-FLAG antibody (diluted at 1/10,000; Sigma) and wash three times with PBS. The cells were then incubated with anti-rabbit IgG-Cy3 (diluted at 1/500; Millipore) with anti-Tubulin-FITC (Sigma) for 3 h at RT. These samples were analyzed using the Leica DM5000B microscope setting.

Analysis of cell morphology

Cells immunostained were randomly chosen and the distance between the center of nuclei and the most distant immunostaining signal from the cell body was measured. We measured 119, 121, 132, 115, 138 and 150 cells for TK(+), T1, rat T2, mouse T2, T3 alpha and T3 beta, respectively. Briefly, captured cell images were superimposed to the concentric circles prepared with Photoshop software with the elemental radius being defined as *r* which is equal to the radius of the nuclear structure. The measurements were then classified into 1*r*–1.5*r*, 1.5*r*–2*r*, 2*r*–2.5*r*, 2.5*r*–3*r*, 3*r*–5*r*, 5*r*–7*r*, 7*r*–10*r*, 10*r*–15*r* and over 15*r*. The percentages of cell number with those categories were calculated and graphed.

Acknowledgments

We thank Drs. Koji Ohira, Masami Kojima, Mikio Hoshino and other members of the Shindan Laboratory for their technical advice and fruitful discussions.

This work was supported by a National Institute of Biomedical Innovation grant (#05-32) to H.K., S.N. and T.I. and a health sciences research grant of nano-1 to S.N.

References

Altar, C.A., DiStefano, P.S., 1998. Neurotrophin trafficking by anterograde transport. Trends. Neurosci. 21, 433–437.

Armanini, M.P., McMahon, S.B., Sutherland, J., Shelton, D.L., Phillips, H.S., 1995. Truncated and catalytic isoforms of trkB are co-expressed in neurons of rat and mouse CNS. Eur. J. Neurosci. 7, 1403–1409.

Barker, P.A., Lomen-Hoerth, C., Gensch, E.M., Meakin, S.O., Glass, D.J., Shooter, E.M., 1993. Tissue-specific alternative splicing generates two isoforms of the trkA receptor. J. Biol. Chem. 268, 15150–15157.

Benito-Gutierrez, E., Garcia-Fernandez, J., Comella, J.X., 2006. Origin and evolution of the Trk family of neurotrophic receptors. Mol. Cell. Neurosci. 31, 179–192.

Bibel, M., Barde, Y.A., 2000. Neurotrophins: key regulators of cell fate and cell shape in the vertebrate nervous system. Genes. Dev. 14, 2919–2937.

Blum, R., Konnerth, A., 2005. Neurotrophin-mediated rapid signaling in the central nervous system: mechanisms and functions. Physiology (Bethesda) 20, 70–78.

Chiaruttini, C., Sonego, M., Baj, G., Simonato, M., Tongiorgi, E., 2008. BDNF mRNA splice variants display activity-dependent targeting to distinct hippocampal laminae. Mol. Cell. Neurosci. 37, 11–19.

Conner, J.M., Lauterborn, J.C., Yan, Q., Gall, C.M., Varon, S., 1997. Distribution of brain-derived neurotrophic factor (BDNF) protein and mRNA in the normal adult rat CNS: evidence for anterograde axonal transport. J. Neurosci. 17, 2295–2313.

Conover, J.C., Erickson, J.T., Katz, D.M., Bianchi, L.M., Poueymirou, W.T., McClain, J., Pan, L., Helgren, M., Ip, N.Y., Boland, P., et al., 1995. Neuronal deficits, not involving motor neurons, in mice lacking BDNF and/or NT4. Nature 375, 235–238.

Coulier, F., Kumar, R., Ernst, M., Klein, R., Martin-Zanca, D., Barbacid, M., 1990. Human trk oncogenes activated by point mutation, in-frame deletion, and duplication of the tyrosine kinase domain. Mol. Cell. Biol. 10, 4202–4210.

Davies, A.M., Minichiello, L., Klein, R., 1995. Developmental changes in NT3 signalling via TrkA and TrkB in embryonic neurons. EMBO J. 14, 4482–4489.

Dugich-Djordjevic, M.M., Ohsawa, F., Hefti, F., 1993. Transient elevation in catalytic trkB mRNA during postnatal development of the rat brain. Neuroreport 4, 1091–1094.

Eide, F.F., Vining, E.R., Eide, B.L., Zang, K., Wang, X.Y., Reichardt, L.F., 1996. Naturally occurring truncated trkB receptors have dominant inhibitory effects on brain-derived neurotrophic factor signaling. J. Neurosci. 16, 3123–3129.

Ernfors, P., Van De Water, T., Loring, J., Jaenisch, R., 1995. Complementary roles of BDNF and NT-3 in vestibular and auditory development. Neuron 14, 1153–1164.
Esteban, P.F., Yoon, H.Y., Becker, J., Dorsey, S.G., Caprari, P., Palko, M.E., Coppola, V., Saragovi, H.U., Randazzo, P.A., Tessarollo, L., 2006. A kinase-deficient TrkC receptor isoform activates Arf6-Rac1 signaling through the scaffold protein tamalin. J. Cell Biol. 173, 291–299.
Fryer, R.H., Kaplan, D.R., Feinstein, S.C., Radeke, M.J., Grayson, D.R., Kromer, L.F., 1996. Developmental and mature expression of full-length and truncated TrkB receptors in the rat forebrain. J. Comp. Neurol. 374, 21–40.
Garner, A.S., Menegay, H.J., Boeshore, K.L., Xie, X.Y., Voci, J.M., Johnson, J.E., Large, T.H., 1996. Expression of TrkB receptor isoforms in the developing avian visual system. J. Neurosci. 16, 1740–1752.
Haapasalo, A., Saarelainen, T., Moshnyakov, M., Arumae, U., Kiema, T.R., Saarma, M., Wong, G., Castren, E., 1999. Expression of the naturally occurring truncated trkB neurotrophin receptor induces outgrowth of filopodia and processes in neuroblastoma cells. Oncogene 18, 1285–1296.
Haapasalo, A., Koponen, E., Hoppe, E., Wong, G., Castren, E., 2001. Truncated trkB.T1 is dominant negative inhibitor of trkB.TK+-mediated cell survival. Biochem. Biophys. Res. Commun. 280, 1352–1358.
Hartmann, M., Brigadski, T., Erdmann, K.S., Holtmann, B., Sendtner, M., Narz, F., Lessmann, V., 2004. Truncated TrkB receptor-induced outgrowth of dendritic filopodia involves the p75 neurotrophin receptor. J. Cell Sci. 117, 5803–5814.
Inoue, T., Tanaka, T., Suzuki, S.C., Takeichi, M., 1998. Cadherin-6 in the developing mouse brain: expression along restricted connection systems and synaptic localization suggest a potential role in neuronal circuitry. Dev. Dyn. 211, 338–351.
Itami, C., Kimura, F., Nakamura, S., 2007. Brain-derived neurotrophic factor regulates the maturation of layer 4 fast-spiking cells after the second postnatal week in the developing barrel cortex. J. Neurosci. 27, 2241–2252.
Jones, K.R., Farinas, I., Backus, C., Reichardt, L.F., 1994. Targeted disruption of the BDNF gene perturbs brain and sensory neuron development but not motor neuron development. Cell 76, 989–999.
Klein, R., Parada, L.F., Coulier, F., Barbacid, M., 1989. trkB, a novel tyrosine protein kinase receptor expressed during mouse neural development. EMBO J. 8, 3701–3709.
Klein, R., Smeyne, R.J., Wurst, W., Long, L.K., Auerbach, B.A., Joyner, A.L., Barbacid, M., 1993. Targeted disruption of the trkB neurotrophin receptor gene results in nervous system lesions and neonatal death. Cell 75, 113–122.
Kryl, D., Yacoubian, T., Haapasalo, A., Castren, E., Lo, D., Barker, P.A., 1999. Subcellular localization of full-length and truncated Trk receptor isoforms in polarized neurons and epithelial cells. J. Neurosci. 19, 5823–5833.
Li, Y.X., Xu, Y., Ju, D., Lester, H.A., Davidson, N., Schuman, E.M., 1998. Expression of a dominant negative TrkB receptor, T1, reveals a requirement for presynaptic signaling in BDNF-induced synaptic potentiation in cultured hippocampal neurons. Proc. Natl. Acad. Sci. U. S. A. 95, 10884–10889.
Liu, X., Ernfors, P., Wu, H., Jaenisch, R., 1995. Sensory but not motor neuron deficits in mice lacking NT4 and BDNF. Nature 375, 238–241.
Luikart, B.W., Nef, S., Shipman, T., Parada, L.F., 2003. In vivo role of truncated trkb receptors during sensory ganglion neurogenesis. Neuroscience 117, 847–858.
Martin-Zanca, D., Barbacid, M., Parada, L.F., 1990. Expression of the trk proto-oncogene is restricted to the sensory cranial and spinal ganglia of neural crest origin in mouse development. Genes. Dev. 4, 683–694.
McMahon, S.B., Armanini, M.P., Ling, L.H., Phillips, H.S., 1994. Expression and coexpression of Trk receptors in subpopulations of adult primary sensory neurons projecting to identified peripheral targets. Neuron 12, 1161–1171.
Middlemas, D.S., Lindberg, R.A., Hunter, T., 1991. trkB, a neural receptor protein-tyrosine kinase: evidence for a full-length and two truncated receptors. Mol. Cell. Biol. 11, 143–153.
Murer, M.G., Yan, Q., Raisman-Vozari, R., 2001. Brain-derived neurotrophic factor in the control human brain, and in Alzheimer's disease and Parkinson's disease. Prog. Neurobiol. 63, 71–124.
Ninkina, N., Grashchuck, M., Buchman, V.L., Davies, A.M., 1997. TrkB variants with deletions in the leucine-rich motifs of the extracellular domain. J. Biol. Chem. 272, 13019–13025.
Ohira, K., Kumanogoh, H., Sahara, Y., Homma, K.J., Hirai, H., Nakamura, S., Hayashi, M., 2005. A truncated tropomyosin-related kinase B receptor, T1, regulates glial cell morphology via Rho GDP dissociation inhibitor 1. J. Neurosci. 25, 1343–1353.
Ohira, K., Funatsu, N., Homma, K.J., Sahara, Y., Hayashi, M., Kaneko, T., Nakamura, S., 2007. Truncated TrkB-T1 regulates the morphology of neocortical layer I astrocytes in adult rat brain slices. Eur. J. Neurosci. 25, 406–416.
Poo, M.M., 2001. Neurotrophins as synaptic modulators. Nat. Rev. Neurosci. 2, 24–32.
Pruunsild, P., Kazantseva, A., Aid, T., Palm, K., Timmusk, T., 2007. Dissecting the human BDNF locus: bidirectional transcription, complex splicing, and multiple promoters. Genomics 90, 397–406.
Reichardt, L.F., 2006. Neurotrophin-regulated signalling pathways. Philos. Trans. R. Soc. Lond. B. Biol. Sci. 361, 1545–1564.
Rose, C.R., Blum, R., Pichler, B., Lepier, A., Kafitz, K.W., Konnerth, A., 2003. Truncated TrkB-T1 mediates neurotrophin-evoked calcium signalling in glia cells. Nature 426, 74–78.
Siegel, G.J., Chauhan, N.B., 2000. Neurotrophic factors in Alzheimer's and Parkinson's disease brain. Brain Res. Brain Res. Rev. 33, 199–227.
Silhol, M., Bonnichon, V., Rage, F., Tapia-Arancibia, L., 2005. Age-related changes in brain-derived neurotrophic factor and tyrosine kinase receptor isoforms in the hippocampus and hypothalamus in male rats. Neuroscience 132, 613–624.
Stoilov, P., Castren, E., Stamm, S., 2002. Analysis of the human TrkB gene genomic organization reveals novel TrkB isoforms, unusual gene length, and splicing mechanism. Biochem. Biophys. Res. Commun. 290, 1054–1065.
Strohmaier, C., Carter, B.D., Urfer, R., Barde, Y.A., Dechant, G., 1996. A splice variant of the neurotrophin receptor trkB with increased specificity for brain-derived neurotrophic factor. EMBO J. 15, 3332–3337.
Wiese, S., Jablonka, S., Holtmann, B., Orel, N., Rajagopal, R., Chao, M.V., Sendtner, M., 2007. Adenosine receptor A2A-R contributes to motoneuron survival by transactivating the tyrosine kinase receptor TrkB. Proc. Natl. Acad. Sci. U. S. A. 104, 17210–17215.
Zuccato, C., Cattaneo, E., 2007. Role of brain-derived neurotrophic factor in Huntington's disease. Prog. Neurobiol. 81, 294–330.

Human Molecular Genetics, 2008, Vol. 17, No. 10 **1482–1496**
doi:10.1093/hmg/ddn037
Advance Access published on February 4, 2008

Aberrant molecular properties shared by familial Parkinson's disease-associated mutant UCH-L1 and carbonyl-modified UCH-L1

Tomohiro Kabuta[1,2,*], Rieko Setsuie[1,2], Takeshi Mitsui[1,3], Aiko Kinugawa[1], Mikako Sakurai[1], Shunsuke Aoki[1], Kenko Uchida[3] and Keiji Wada[1,*]

[1]Department of Degenerative Neurological Diseases, National Institute of Neuroscience, National Center of Neurology and Psychiatry, 4-1-1 Ogawahigashi, Kodaira, Tokyo 187-8502, Japan, [2]The Japan Health Sciences Foundation, 13-4 Nihonbashi Kodenma, Chuo-ku, Tokyo 103-0001, Japan and [3]Department of Electrical Engineering and Bioscience, Waseda University, Tokyo 169-8555, Japan

Received January 8, 2008; Revised and Accepted January 30, 2008

Parkinson's disease (PD) is a neurodegenerative disorder characterized by loss of dopaminergic neurons. The I93M mutation in ubiquitin C-terminal hydrolase L1 (UCH-L1) is associated with familial PD, and we have previously shown that the I93M UCH-L1-transgenic mice exhibit dopaminergic cell loss. Over 90% of neurodegenerative diseases, including PD, occur sporadically. However, the molecular mechanisms underlying sporadic PD as well as PD associated with I93M UCH-L1 are largely unknown. UCH-L1 is abundant (1–5% of total soluble protein) in the brain and is a major target of oxidative/carbonyl damage associated with sporadic PD. As well, abnormal microtubule dynamics and tubulin polymerization are associated with several neurodegenerative diseases including frontotemporal dementia and parkinsonism linked to chromosome 17. Here we show that familial PD-associated mutant UCH-L1 and carbonyl-modified UCH-L1 display shared aberrant properties: compared with wild-type UCH-L1, they exhibit increased insolubility and elevated interactions with multiple proteins, which are characteristics of several neurodegenerative diseases-linked mutants. Circular dichroism analyses suggest similar structural changes in both UCH-L1 variants. We further report that one of the proteins interacting with UCH-L1 is tubulin, and that aberrant interaction of mutant or carbonyl-modified UCH-L1 with tubulin modulates tubulin polymerization. These findings may underlie the toxic gain of function by mutant UCH-L1 in familial PD. Our results also suggest that the carbonyl modification of UCH-L1 and subsequent abnormal interactions of carbonyl-modified UCH-L1 with multiple proteins, including tubulin, constitute one of the causes of sporadic PD.

INTRODUCTION

Parkinson's disease (PD) is the most common neurodegenerative movement disorder and is characterized by progressive cell loss confined mostly to dopaminergic neurons in the substantia nigra pars compacta. The I93M mutation in ubiquitin C-terminal hydrolase L1 (UCH-L1) was reported in a German family with dominantly inherited PD (1). To assess the correlation of the I93M mutation and pathogenesis of PD, we have previously generated UCH-L1^{I93M}-transgenic mice. These mice exhibited progressive dopaminergic cell loss in the substantia nigra (2), suggesting that the I93M mutation in UCH-L1 is a causative mutation for PD. The S18Y polymorphism in UCH-L1 has been reported to be associated with decreased risk of PD (3). However, it has also been reported that S18Y is not associated with risk of PD (4).

UCH-L1 is abundant (1–5% of total soluble protein) in the brain (5) and is thought to hydrolyse polymeric ubiquitin and ubiquitin conjugates to monoubiquitin (6). UCH-L1 has also been reported to act as a ubiquitin ligase *in vitro* (7). In

*To whom correspondence should be addressed. Tel: +81 423461715; Fax: +81 423461745; Email: kabuta@ncnp.go.jp (T.K.); wada@ncnp.go.jp (K.W.)

addition to these enzymatic activities, we have found that UCH-L1 binds to and stabilizes monoubiquitin in neurons (8). Our previous studies using circular dichroism (CD) and small-angle neutron scattering strongly suggested that the I93M mutation in UCH-L1 alters the conformation of UCH-L1 (9,10). We have previously shown that mice deficient in UCH-L1 do not exhibit obvious dopaminergic cell loss, in contrast to UCH-L1^{I93M}-transgenic mice (2,8,11), suggesting that a loss or decrease in the level of UCH-L1 is not the main cause of PD, and that UCH-L1^{I93M}-associated PD is caused by an acquired toxicity. Thus, although the hydrolase activity of UCH-L1^{I93M} is decreased (1,9), this decreased activity may not be a major cause of PD.

Increased oxidative stress is associated with neurodegenerative diseases (12,13). In sporadic PD brains, UCH-L1 is a major target of carbonyl formation (12), which is the most widely used marker for oxidative damage to proteins. UCH-L1 has also been identified as a component of several inclusion bodies characteristic of neurodegenerative diseases, including Lewy bodies (14). These findings suggest that UCH-L1 and its modification by carbonyl formation are involved in the cause of sporadic PD. Despite the fact that the majority of PD cases occur sporadically, the molecular mechanisms underlying the causes of sporadic PD, as well as UCH-L1^{I93M}-associated PD, are largely unknown. Moreover, the biochemical properties of UCH-L1^{I93M} and carbonyl-modified UCH-L1 in mammalian cells, such as their protein interactions or detergent insolubility (i.e. the amount of a protein in the insoluble fraction), are poorly understood.

In this study, we analyzed the molecular properties of carbonyl-modified UCH-L1 and UCH-L1^{I93M} and elucidated novel properties of UCH-L1 variants, including protein interactions. We show that carbonyl-modified UCH-L1 and UCH-L1^{I93M} share common properties. Our findings provide novel insights into understanding the mechanisms underlying the toxic gain of function by mutant UCH-L1 and suggest that oxidative stress and subsequent protein interactions of carbonyl-modified UCH-L1 constitute one of the causes of sporadic PD. We also discuss the possible involvement of oxidative modifications of UCH-L1 in other neurodegenerative diseases.

RESULTS

Disease-associated mutants including UCH-L1^{I93M} display aberrant insolubility

Aberrantly increased insolubility compared with wild-type protein is a common biochemical feature of several mutant proteins associated with neurodegenerative diseases: for example, mutant α-synuclein associated with familial PD (15), mutant SOD1 associated with familial amyotrophic lateral sclerosis (ALS) (16,17) and mutant tau associated with frontotemporal dementia and parkinsonism linked to chromosome 17 (18). Although we have previously shown that the insolubility of UCH-L1 in the UCH-L1^{I93M}-transgenic mouse brain is increased compared with that in wild-type mouse (2), the insolubility of UCH-L1^{I93M} itself has been unclear. We observed that pathogenic α-synuclein and SOD1 mutant proteins exhibit increased detergent insolubility in mammalian cells compared with wild-type proteins (Fig. 1A and B). The insolubility of UCH-L1^{I93M} was examined under the same experimental conditions, in which the causative mutants are distinguishable from wild-type proteins. We found that, in dopaminergic SH-SY5Y cells, the protein level of UCH-L1^{I93M} in the insoluble fraction was markedly higher than the levels of UCH-L1^{WT}, UCH-L1^{S18Y}, UCH-L1^{D30K}, which lacks hydrolase activity and binding affinity for ubiquitin (8), and UCH-L1^{C90S}, which lacks hydrolase activity but maintains binding affinity for ubiquitin (8) (Fig. 1C). There was no notable difference among the soluble protein levels (Fig. 1C). The formation of high molecular weight aggregates, which is also a common feature of several mutants, was observed almost exclusively in the insoluble fraction with UCH-L1^{I93M} (Fig. 1C), consistent with the report that UCH-L1^{I93M} produced more aggresomes than UCH-L1^{WT} (19). Increased insolubility of UCH-L1^{I93M} and UCH-L1$^{S18Y/I93M}$ and an increase in the amounts of aggregates specific for these proteins were observed in COS-7 cells (Fig. 1D; Supplementary Material, Fig. S1A), which express very low levels of endogenous UCH-L1. These results demonstrate that UCH-L1^{I93M} shares common features with several mutant proteins linked to neurodegenerative diseases, thus, further supporting the idea that the I93M mutation in UCH-L1 is a causative mutation for PD. Our results also suggest that the insolubility of UCH-L1 is independent of monoubiquitin-binding.

UCH-L1^{I93M} abnormally interacts with multiple proteins

Although increased insolubility is a common characteristic of several mutant proteins associated with neurodegenerative diseases, and this may play a role in the neurotoxicity of the mutant proteins, accumulating evidence suggests that a soluble mutant is the main cause of neurodegeneration (20,21). Studies of dominantly inherited neurodegenerative disease-linked mutants strongly suggest that abnormal physical interactions of the mutant proteins with other proteins constitute a cause of disease (22–26). Hence, we next examined the effect of the I93M mutation on the protein interactions of soluble UCH-L1 using a co-immunoprecipitation (coIP) assay. Silver staining of immunoprecipitant revealed that UCH-L1^{WT} interacts with multiple proteins over 30 kDa (Fig. 1E). We found that the amount of each protein interacting with UCH-L1^{I93M} is mostly higher than the amount interacting with UCH-L1^{WT} or other UCH-L1 variants (Fig. 1F; Supplementary Material, Fig. S1B). Monoubiquitin binding of UCH-L1^{I93M} was decreased compared with that of UCH-L1^{WT} (Fig. 1G), consistent with the decreased hydrolase activity of UCH-L1^{I93M} (1,9). However, the cellular monoubiquitin level in cells expressing UCH-L1^{I93M} was not changed compared with that in cells expressing UCH-L1^{WT} (Fig. 1G). Since UCH-L1^{I93M}-associated PD is presumably caused by an acquired toxicity, the toxic function of UCH-L1^{I93M} may not be mainly mediated by a decreased interaction with monoubiquitin, but rather by aberrantly elevated interactions with multiple other proteins.

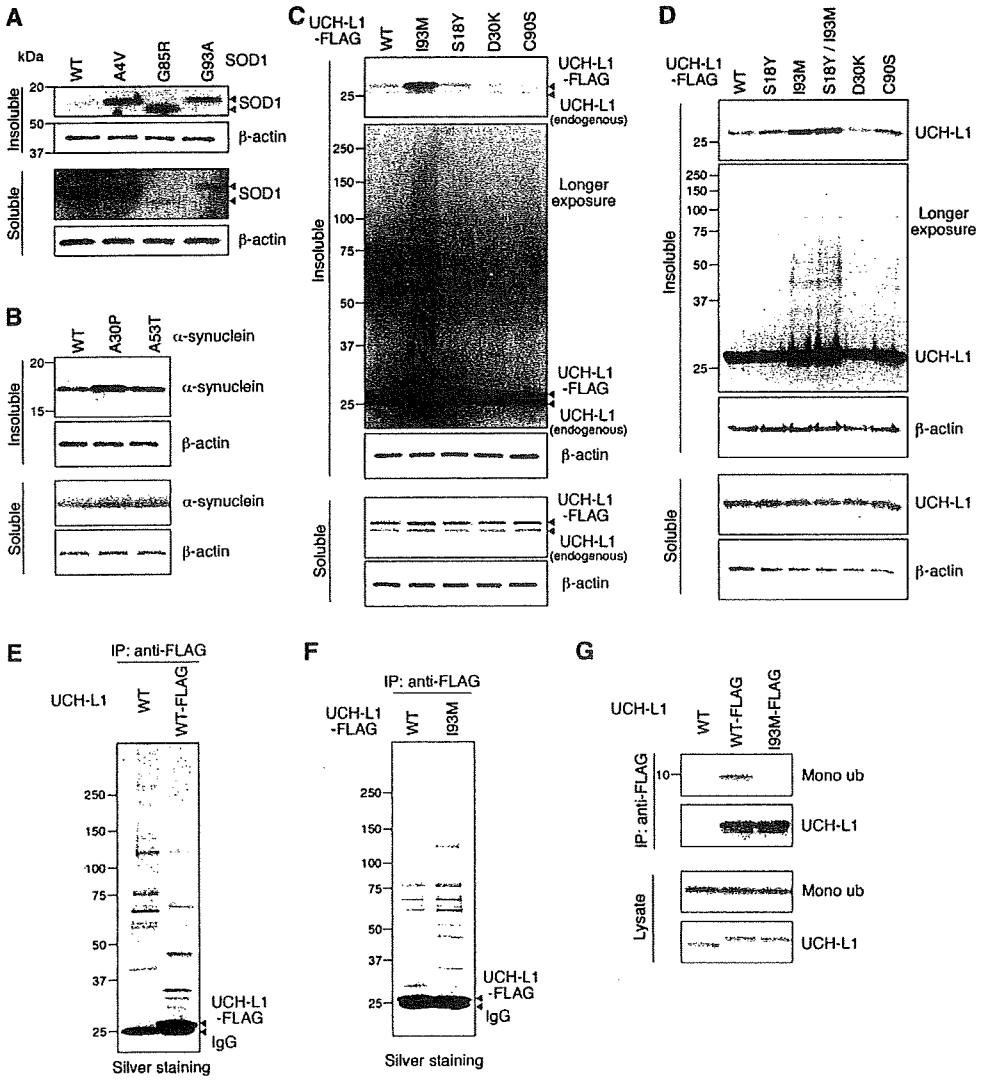

Figure 1. Aberrant biochemical properties of mutant I93M UCH-L1. [(**A**)–(**D**)] SH-SY5Y (A) and (C), Neuro2a (B) and COS-7 cells (D) were transfected with the indicated constructs. Forty-eight hours after transfection, soluble and insoluble fractions were prepared and analyzed by immunoblotting. [(**E**)–(**G**)] COS-7 cells were transfected with the indicated constructs. Cell lysates were immunoprecipitated using anti-FLAG antibody and analyzed by silver staining [(E) and (F)] or by immunoblotting (G). In the presence of FLAG-tagged UCH-L1, UCH-L1-interacting proteins were co-immunoprecipitated with UCH-L1 [(E), lane 2], whereas in the absence of FLAG-tagged UCH-L1, proteins were non-specifically precipitated with anti-FLAG beads [(E), lane 1]. Mono ub, monoubiquitin (G).

Carbonyl-modified UCH-L1 exhibits aberrant properties common to UCH-L1^{I93M}

In the brains of sporadic PD patients, UCH-L1 is a major target of carbonyl formation (12). Carbonyl groups can be introduced into proteins *in vivo* mainly by reactions with 2-alkenals, 4-hydroxy-2-alkenals (HAE) or ketoaldehydes, which are endogenous aldehydic products formed by lipid peroxidation or glycooxidation (27,28). Protein carbonyls can also be produced by metal-catalyzed reactions with H_2O_2 *in vitro* (28,29). To analyze the biochemical properties of carbonyl-modified UCH-L1, we used several carbonyl compounds or H_2O_2 to modify UCH-L1. We have previously reported that UCH-L1 is modified by 4-hydroxy-2-nonenal (HNE) *in vitro* (9). In COS-7 cells transfected with UCH-L1^{WT}, UCH-L1 was modified by physiological concentrations of HNE (10–100 μM) (9) or 4-hydroxy-2-hexenal (HHE) in a dose-dependent manner (Fig. 2A and B; Supplementary Material, Fig. S1C). Carbonyl modification of UCH-L1 was also detected when cells were treated with 100 μM 2-propenal (Fig. 2A), but not with 100 or 500 μM methylglyoxal, 100 or 500 μM malondialdehyde, both of which are ketoaldehydes, or 0.1 or 1 mM H_2O_2 (data not shown). Thus, carbonyl-modified UCH-L1 can be produced by reactions with HAE or 2-alkenals in mammalian cells.

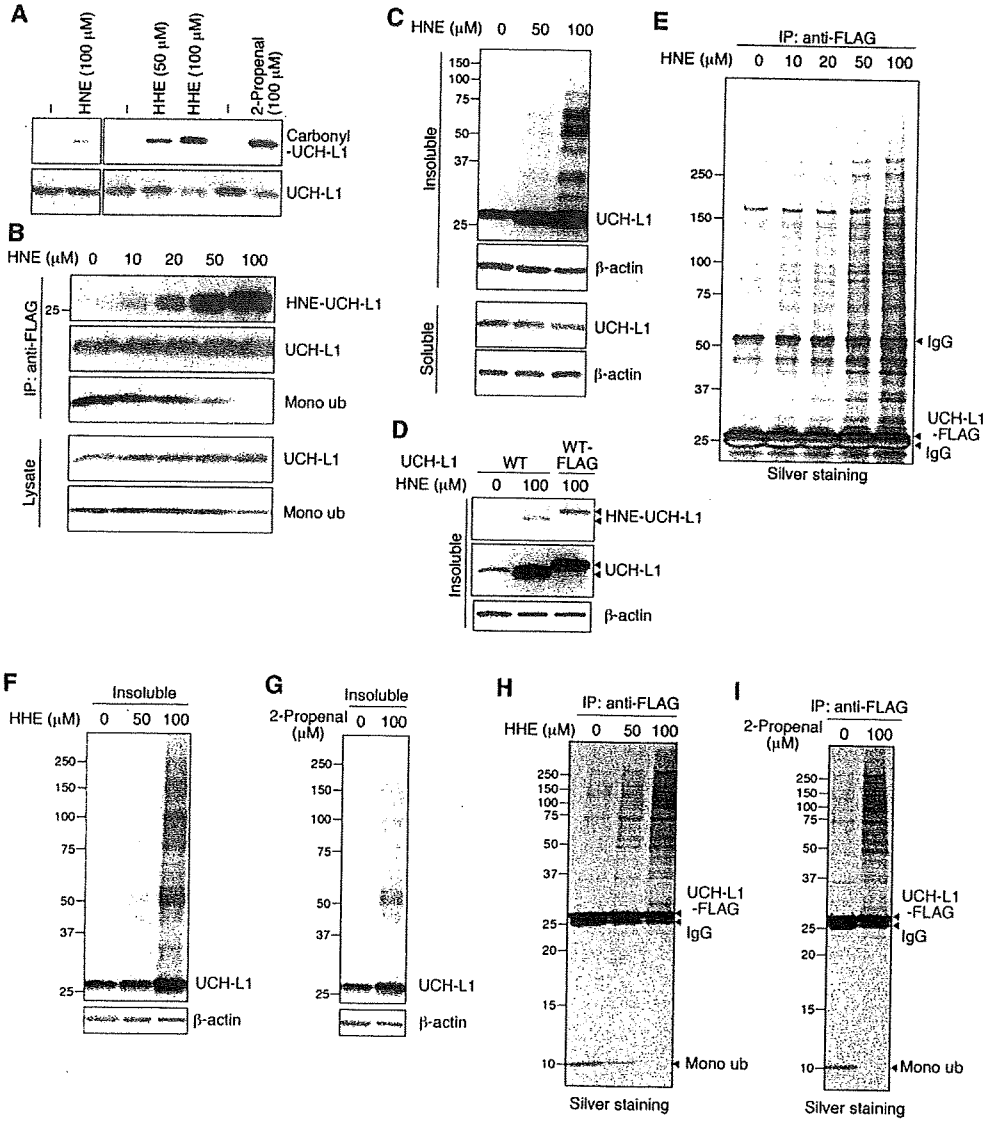

Figure 2. Abnormal biochemical properties of carbonyl-modified UCH-L1. **(A)** COS-7 cells transfected with FLAG-tagged UCH-L1^{WT} were treated with or without the indicated concentrations of carbonyl compounds for 90 min, and immunoprecipitation was performed using anti-FLAG antibody. To detect carbonyl-modified UCH-L1, immunoprecipitants were derivatized with DNPH and immunoblotted using anti-DNP or anti-UCH-L1 antibodies. [**(B)**, **(E)**, **(H)** and **(I)**] COS-7 cells transfected with FLAG-tagged UCH-L1^{WT} were treated with the indicated concentrations of HNE [(B) and (E)], HHE (H) or 2-propenal (I) for 90 min, and immunoprecipitation was performed using anti-FLAG antibody. Immunoprecipitants were analyzed by immunoblotting or by silver staining. [**(C)**, **(F)** and **(G)**] COS-7 cells transfected with FLAG-tagged UCH-L1^{WT} were treated with the indicated concentrations of HNE (C), HHE (F) or 2-propenal (G). Soluble and insoluble fractions were analyzed by immunoblotting. **(D)** COS-7 cells transfected with the indicated constructs were treated with or without HNE, and insoluble fractions were prepared. Immunoblotting shows that the insoluble UCH-L1 that is accumulated upon HNE treatment is modified by HNE.

Interestingly, carbonyl-modified UCH-L1 and UCH-L1^{I93M} exhibit common biochemical properties: ubiquitin binding of HNE-modified UCH-L1 was decreased (Fig. 2B), and both the insolubility of HNE-modified UCH-L1 and the interactions of HNE-modified UCH-L1 with proteins over 30 kDa were increased, compared with those of UCH-L1^{WT} (Fig. 2C–E). HHE and 2-propenal had similar effects to HNE (Fig. 2F–I). Treatment of cells with 100 μM H_2O_2, methylglyoxal or malondialdehyde had no effect on the insolubility of UCH-L1 or the interactions of UCH-L1 with other proteins (data not shown). Consistent with the report that UCH-L1 is a major target of carbonyl formation in the brains of sporadic PD patients (12), UCH-L1 is a major target of carbonyl modification in cells treated with HNE (Fig. 3A). We used the EF1 promoter to yield abundant expression of UCH-L1 in this experiment, since the amount of UCH-L1 is 1–5% of

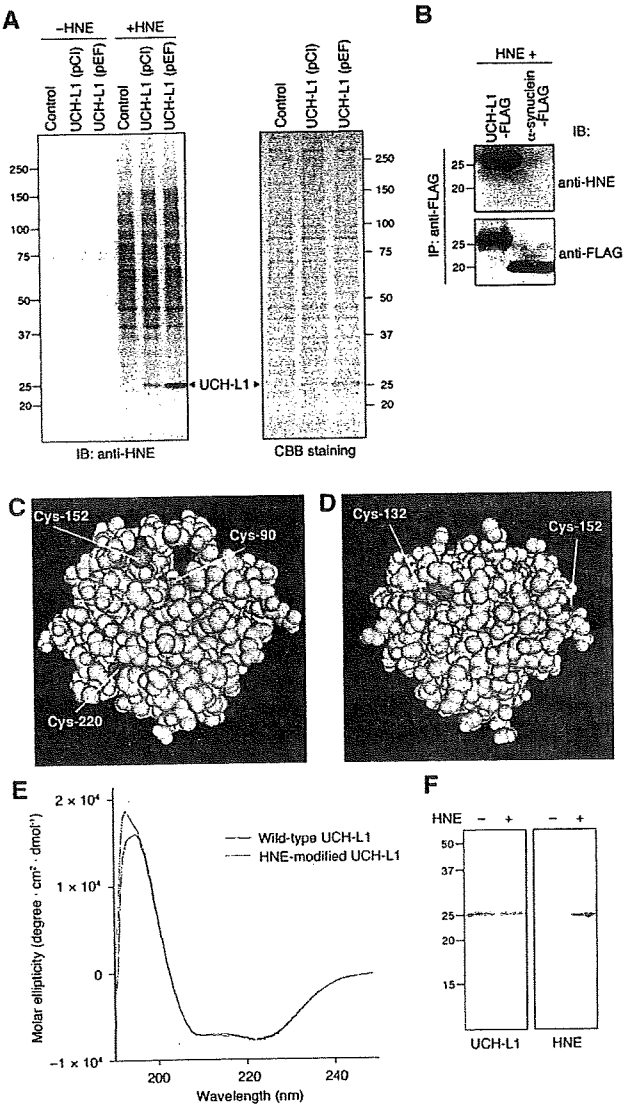

Figure 3. Susceptibility of UCH-L1 to HNE modification and structural properties of UCH-L1 variants. (**A**) COS-7 cells transfected with the indicated constructs were treated with or without 100 μM HNE and analyzed by immunoblotting and CBB staining. (**B**) COS-7 cells transfected with the indicated constructs were treated with 100 μM of HNE, and immunoprecipitation was performed using anti-FLAG antibody. Immunoprecipitants were analyzed by immunoblotting. [(**C**) and (**D**)] Structural model for human UCH-L1. Cys-90, Cys-152 and Cys-220 sidechains are shown in magenta, and backbones are shown in blue (C), using Cn3D software (version 4.1) and NCBI's structural model (mmdbId:38174). Cys-132 and Cys-152 sidechains are shown in magenta, and backbones are shown in blue (D). (**E**) CD spectra (mean residue ellipticity) for recombinant human UCH-L1 proteins. Wild-type UCH-L1 is shown in red and HNE-modified UCH-L1 in blue. (**F**) HNE modification of the recombinant UCH-L1 used in (E) was analyzed by immunoblotting. Modification of UCH-L1 by HNE was detected.

soluble protein in the brain (5). These results suggest that the carbonyl-modified UCH-L1 in sporadic PD brains functions as a causative factor for disease in a similar manner to UCH-L1^{I93M}.

Cys-90 and Cys-152 of UCH-L1 are targets for HAE modification

The appearance of HNE-modified proteins in nigral neurons has been shown to be associated with sporadic PD (30,31). Therefore, we next determined the HNE-modified amino acid residues of UCH-L1 that regulate its insolubility and protein interactions. HNE can form covalent cross-links with cysteine, lysine and histidine residues in proteins (28). To test the specificity of HNE modification in mammalian cells, we used cells transfected with α-synuclein, which contains no cysteine residues. HNE modification of α-synuclein was not detected when cells were treated with 100 μM HNE (Fig. 3B). These results suggest that among the amino acid residues of UCH-L1, cysteine residues are the primary target for HAE. We speculated that Cys-90 is accessible to HAE, since it is accessible to ubiquitin. Using the three-dimensional structure of human UCH-L1 (32), we observed that not only Cys-90 but also Cys-132 and Cys-152 are located on the surface of the protein (Fig. 3C and D). Thus, we tested the insolubility and protein interactions using C90S, C132S and C152S UCH-L1 mutant proteins. We also used C220S UCH-L1 as a control. We found that the C152S mutant bound to monoubiquitin in both HNE-treated cells and untreated cells (Fig. 4A). UCH-L1^{C90S} did not exhibit notably increased insolubility upon HNE-treatment compared with UCH-L1^{WT} (1.3-fold increase in UCH-L1^{C90S}, 2.5-fold increase in UCH-L1^{WT}) (Fig. 4B). The amount of proteins over 30 kDa interacting with UCH-L1^{C90S} was markedly lower than that interacting with UCH-L1^{WT} when cells were treated with HNE (Fig. 4C). Similar results were obtained when cells were treated with HHE (Fig. 4E and F; Supplementary Material, Fig. S1D). Mutations at Cys-132 and Cys-220 had no effect on protein insolubility or interactions (Fig. 4A–C). Consistent with these results, HNE modification of C90S and C152S mutants was decreased compared with that of UCH-L1^{WT} when cells were treated with HNE (~40 and 60% decrease, respectively) (Fig. 4D). These results indicate that HAE modification of UCH-L1 at Cys-90 increases the insolubility and interactions of UCH-L1, and modification of Cys-152 reduces monoubiquitin binding. The level of HNE modification of UCH-L1^{I93M} upon HNE-treatment was markedly lower than that of UCH-L1^{WT} (Fig. 4G). Since the location of Cys-90 is close to Ile-93 (Supplementary Material, Fig. S2), it is possible that the I93M mutation and HAE modification at Cys-90 cause similar structural changes in UCH-L1.

HNE modification causes structural changes in UCH-L1

To address the structural changes in carbonyl-modified UCH-L1, we used CD spectroscopy to estimate the secondary structure. We have previously shown that, compared with UCH-L1^{WT}, the I93M mutant displays lower ellipticity around 195 nm, suggesting a decreased α-helix content, and an increase in the content of β-sheet (9,10). Relative to wild-type protein, HNE-modified UCH-L1 also displayed a lower peak around 190–195 nm (Fig. 3E and F). The relative proportions of α-helix, β-sheet and other secondary structural features in these proteins were estimated from mean residue ellipticity data. HNE-modified UCH-L1 also exhibited

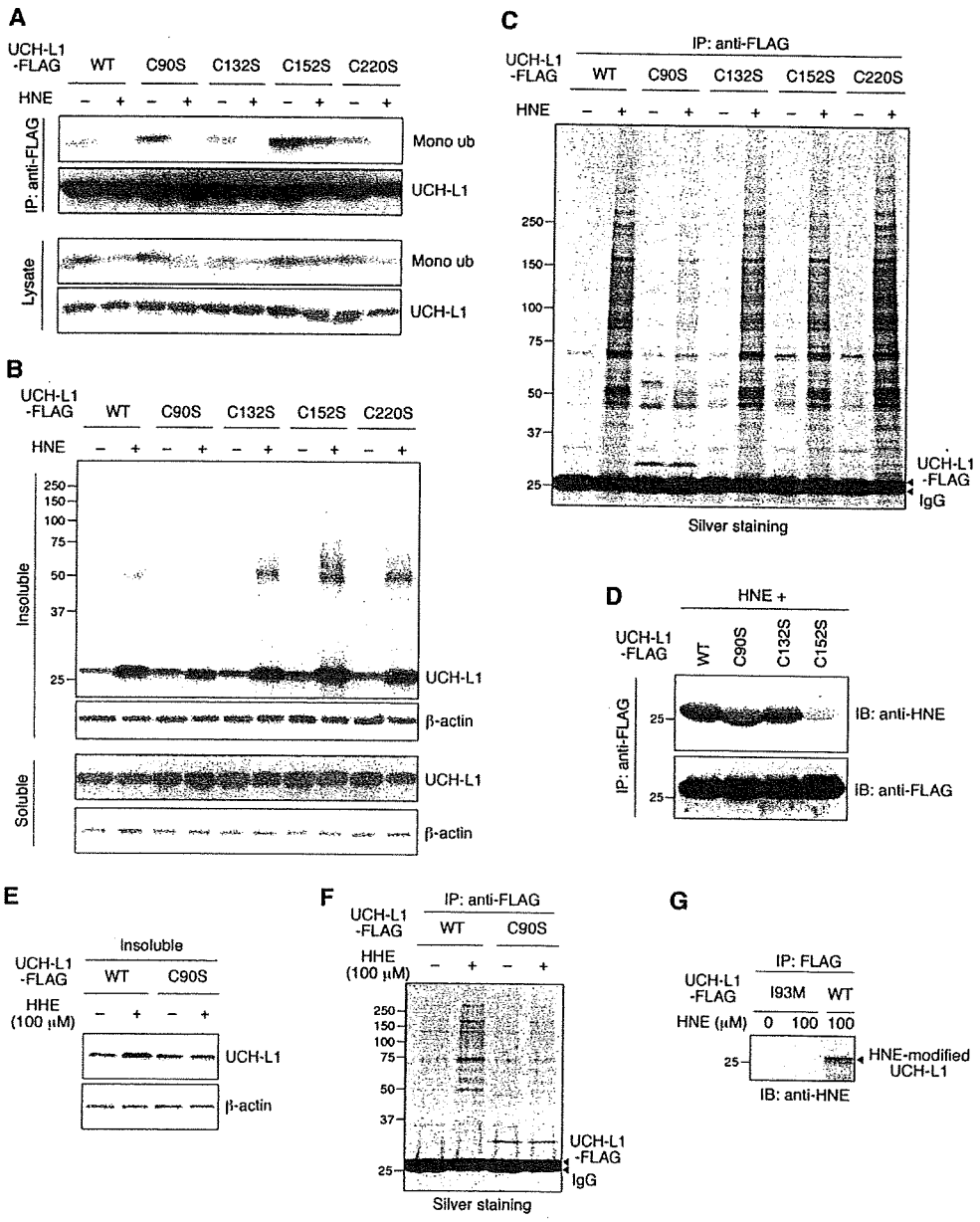

Figure 4. Cysteine residues of UCH-L1 modified by HAE. [**(A)**, **(C)**, **(D)**, **(F)** and **(G)**] COS-7 cells transfected with the indicated constructs were treated with or without 100 μM HNE or HHE. Immunoprecipitation was performed using anti-FLAG antibody, and immunoprecipitants were analyzed by immunoblotting or by silver staining. [**(B)** and **(E)**] COS-7 cells transfected with the indicated constructs were treated with or without 100 μM HNE or HHE. Soluble and insoluble fractions were analyzed by immunoblotting.

decreased α-helix content, and an increase in the content of β-sheet compared with UCH-L1^{WT} (42.9% α-helix, 20.9% β-sheet, 20.6% β-turn and 15.7% random for UCH-L1^{WT}, and 34.0% α-helix, 27.3% β-sheet, 22.3% β-turn and 16.4% random for HNE-modified UCH-L1). These results suggest that UCH-L1^{I93M} and carbonyl-modified UCH-L1 adopt a similar aberrant structure.

The ALS-linked mutation in SOD1 increases its hydrophobicity, which may promote aberrant interactions of SOD1 with other cellular constituents (33). However, the interactions of UCH-L1^{I93M} or HNE-modified UCH-L1 with hydrophobic beads were not altered relative to those of UCH-L1^{WT} (data not shown), indicating that the I93M mutation and HNE modification of UCH-L1 do not increase its hydrophobicity. Considering the fact that unnatural β-sheet proteins readily become insoluble or form further β-hydrogen-bonding with other β-strands they encounter (34), our results suggest that the increased insolubility and protein interactions of abnormal UCH-L1 are due to the increased β-sheet content of UCH-L1.

UCH-L1 physically interacts with tubulin

To understand the molecular mechanism underlying toxic gain of function by UCH-L1, we attempted to identify UCH-L1^{I93M}-interacting proteins by coIP assay and subsequent LC-MS/MS analysis (Fig. 5A). A database search of the peptide sequences obtained identified α-tubulin as a UCH-L1^{I93M}-interacting protein (Supplementary Material, Table S1). The interaction between UCH-L1 and endogenous α-tubulin was confirmed with transiently expressed UCH-L1 (Fig. 5B and C). The interaction of UCH-L1^{I93M} with α-tubulin was increased compared with that of UCH-L1^{WT} (Fig. 5B). We detected the interaction of endogenous α-tubulin with endogenous UCH-L1 using Neuro2a cells (Fig. 5D). Tubulin is composed of a heterodimer of α- and β-tubulin, and we confirmed, using native-PAGE, that tubulin exists as a heterodimer in cell lysates in coIP experimental conditions (data not shown), indicating that UCH-L1 interacts with tubulin. Indeed, β-tubulin was also precipitated with UCH-L1 (Supplementary Material, Fig. S3). In contrast to tubulin, interaction of β-actin with UCH-L1 was not detected (Fig. 5C). To test whether UCH-L1 directly interacts with tubulin, we performed pull-down assay using recombinant UCH-L1 and purified tubulin. Direct interaction of UCH-L1 with tubulin was observed (Fig. 5E).

Since the interactions between UCH-L1 and proteins over 30 kDa are increased by carbonyl modification or I93M mutation of UCH-L1, we tested the effects of HAE on the interaction of UCH-L1 with tubulin. We found that HAE modification of UCH-L1 promotes interactions between UCH-L1 and tubulin (Fig. 5F, G and I). In addition, a coIP assay using C90S, C132S and C152S UCH-L1 mutants showed less binding of UCH-L1^{C90S} to tubulin than UCH-L1^{WT} did, when cells were treated with HNE or HHE (Fig. 5G–I), indicating that the increased interaction of UCH-L1 with tubulin is caused by the HAE modification of Cys-90 of UCH-L1. These results are consistent with the results showing that the HAE modification of Cys-90 of UCH-L1 promotes the interaction of UCH-L1 with multiple proteins. The I93M mutation and HNE modification of UCH-L1 also promote direct interactions between UCH-L1 and tubulin (data not shown). Thus, UCH-L1^{I93M} and HNE-UCH-L1 also exhibit common biochemical properties with respect to the interactions with tubulin.

Both UCH-L1^{I93M} and carbonyl-modified UCH-L1 aberrantly promote tubulin polymerization

Microtubules are dynamic polymers composed of tubulin that continuously grow and shorten through tubulin addition and loss at the microtubule ends. Microtubule-stabilizing agents such as paclitaxel, which promote tubulin polymerization and suppress microtubule dynamics, are effective chemotherapeutic agents for the treatment of many cancers. However, neuropathy is a major adverse effect of microtubule-stabilizing agents-based chemotherapy (35). Paclitaxel induces apoptosis in cortical neurons by a mechanism independent of its cell cycle effects, because postnatal cortical neurons are postmitotic (36). These findings indicate that tubulin polymerization must be tightly regulated for neurons to function and remain viable. Furthermore, abnormal microtubule dynamics and tubulin polymerization are associated with several neurodegenerative diseases including frontotemporal dementia and parkinsonism linked to chromosome 17 (37,38). Therefore, we examined the effects of UCH-L1^{WT}, UCH-L1^{I93M} and HNE-UCH-L1 on tubulin polymerization using an *in vitro* assay. Interestingly, both UCH-L1^{I93M} and HNE-UCH-L1 promote tubulin polymerization, although UCH-L1^{WT} had almost no effect on it (Fig. 6A and B). Promotion of tubulin polymerization may result in a stabilization of microtubules because of the dynamic instability of microtubules. To test whether abnormal UCH-L1 also promotes tubulin polymerization in mammalian cells, we analyzed the amounts of soluble, polymeric and total tubulin in cells expressing UCH-L1^{I93M}. Although transient expression of UCH-L1^{I93M} had no effect on the amount of total tubulin (Fig. 5B), cells stably expressing UCH-L1^{I93M} contained increased amount of total tubulin compared with control cells or cells expressing other UCH-L1 variants (Fig. 6C). Consistent with the *in vitro* polymerization assay, the amount of polymeric tubulin was increased in cells expressing UCH-L1^{I93M}, whereas the amount of soluble tubulin was not (~1.4 and 1.0-fold increase, respectively, compared with the amount of tubulin in cells expressing UCH-L1^{WT}) (Fig. 6D). The amount of β-actin was not affected by the expression of UCH-L1 variants (Fig. 6C and D), also consistent with the results showing that UCH-L1 does not interact with β-actin. We did not detect specific interaction of UCH-L1 with polymerized tubulin (Fig. 6E), indicating that UCH-L1 may not interact with microtubules, although the possibility is not excluded that they can interact under certain conditions or at a limited number of sites such as the microtubule ends.

Since D30K and C90S mutations had no effect on the interaction of UCH-L1 and tubulin (Fig. 5B), we speculated that the tubulin-binding region of UCH-L1 is different from ubiquitin-binding region. To elucidate the amino acid residues of UCH-L1 involved in the interaction with tubulin and to show that modulation of tubulin polymerization is caused by the increased interaction of UCH-L1 with tubulin, we made a series of alanine substitutions of basic and acidic residues located on the surface of UCH-L1 and performed coIP assays using these mutants (Fig. 7A; Supplementary Material, Fig. S3). The R63A and H185A mutants displayed increased interactions with tubulin (Fig. 7A), indicating that Arg-63 and His-185, which are distinct from the ubiquitin-binding region (Fig. 7B), are involved in this interaction. The increased interactions of R63A and H185A UCH-L1 with tubulin may be caused by altered ionic interactions. In contrast to the I93M mutant or HNE-UCH-L1, the R63A mutant caused a decrease in tubulin polymerization (Fig. 7C). Although UCH-L1^{R63A} has opposite effects to the I93M mutant or HNE-UCH-L1, it also modulated tubulin polymerization. Thus, modulation of tubulin polymerization by UCH-L1 variants is caused by the abnormally increased interaction of UCH-L1 with tubulin.

From our results, we hypothesized that UCH-L1^{I93M}-associated neurodegeneration or PD is at least partly mediated by aberrant tubulin polymerization. Therefore, we tested the effects of UCH-L1^{I93M} and paclitaxel on neuronal cell death using differentiated Neuro2a cells, which

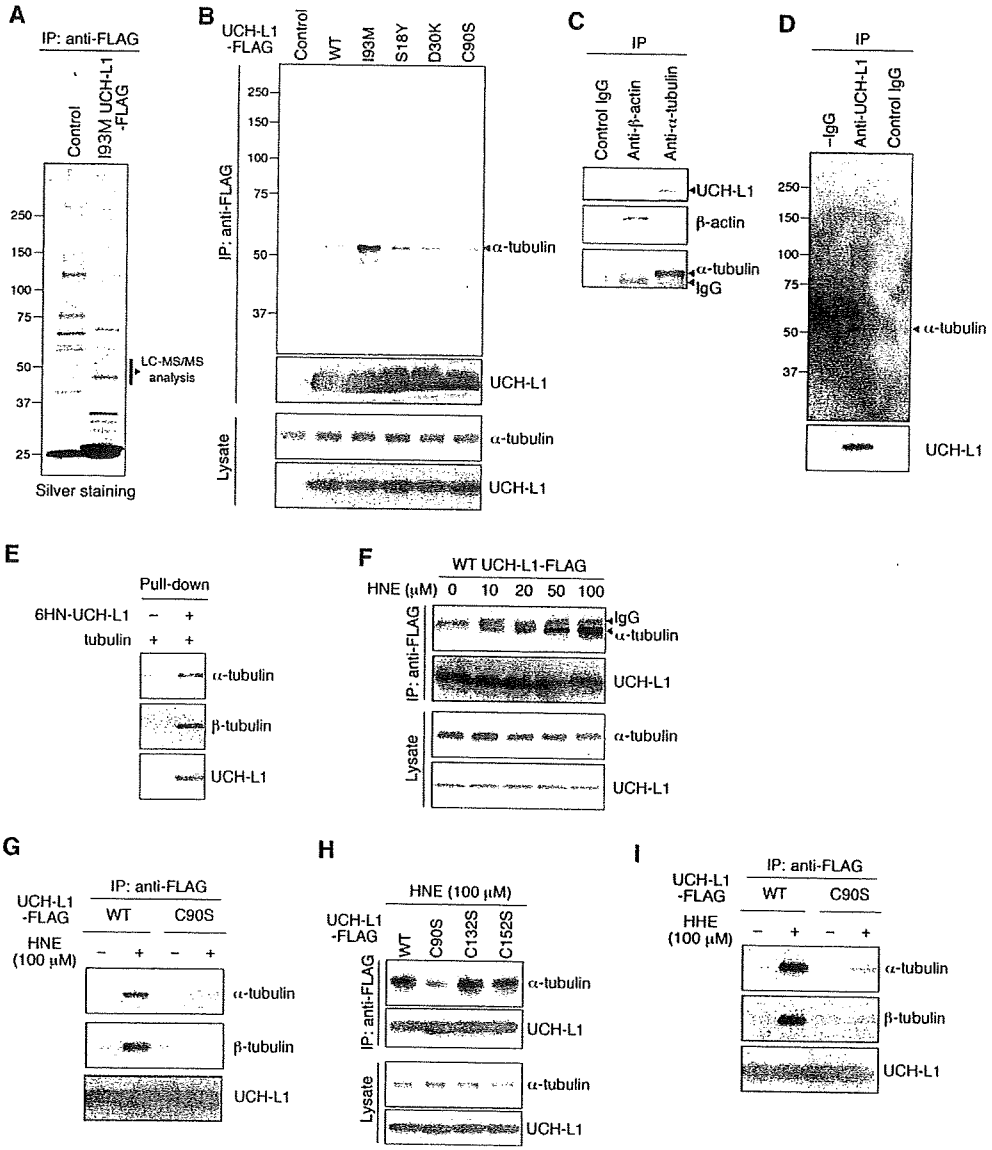

Figure 5. Physical interactions of UCH-L1 with tubulin. (**A**) Lysates of HeLa cells transfected with the indicated constructs (control: GFP) were immunoprecipitated with anti-FLAG antibody and analyzed by silver staining. Proteins ~50 kDa in size were subjected to LC-MS/MS analysis. (**B**) Lysates of COS-7 cells transfected with the indicated constructs (control: empty vector) were immunoprecipitated with anti-FLAG antibody and analyzed by immunoblotting. (**C**) Lysates of NIH-3T3 cells stably expressing FLAG-HA-tagged UCH-L1 were immunoprecipitated with the indicated antibodies and analyzed by immunoblotting. (**D**) Lysates of Neuro2a cells were immunoprecipitated with control IgG or anti-UCH-L1 antibody and analyzed by immunoblotting. –IgG, without IgG. (**E**) A pull-down assay was performed using the indicated purified proteins. [(**F**)–(**I**)] COS-7 cells transfected with the indicated constructs were treated with the indicated concentrations of HNE. Lysates were immunoprecipitated with anti-FLAG antibody and analyzed by immunoblotting.

have been used to assess the toxicity of mutant proteins linked to neurodegenerative diseases (17,39,40). We confirmed that paclitaxel does not interfere with the interaction between UCH-L1 and tubulin (data not shown). Treatment of cells with 5 μM paclitaxel slightly but significantly elevated cell death in cells expressing UCH-L1^{I93M}, but had no effect in cells expressing UCH-L1^{WT} (Fig. 6F). This indicated that the toxicity of UCH-L1^{I93M} may be at least in part mediated by aberrant microtubule dynamics or tubulin polymerization.

Given that tightly regulated tubulin polymerization is necessary for neurons to be viable, our findings strongly suggest that aberrant tubulin polymerization caused by UCH-L1^{I93M} partly underlies the toxic gain of function of mutant UCH-L1, and that carbonyl-modified UCH-L1 also functions as a toxic protein in neurons. We propose that interactions of mutant or carbonyl-modified UCH-L1 with other proteins, including tubulin, constitute one of the causes of not only familial PD, but also sporadic PD (Fig. 7D).

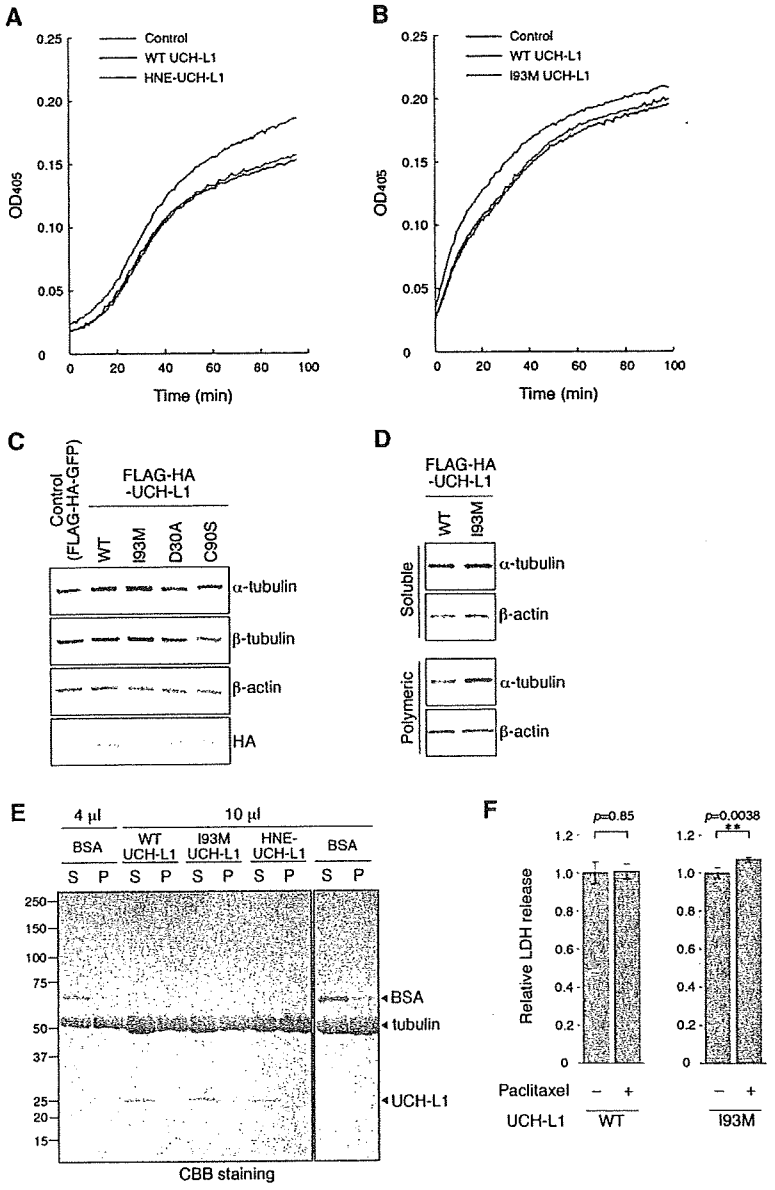

Figure 6. Effects of the I93M mutation and HNE modification of UCH-L1 on tubulin polymerization. [(**A**) and (**B**)] A tubulin polymerization assay was performed in the absence (control) or in the presence of recombinant UCH-L1. The assays were performed at least three times; representative results are shown. [(**C**) and (**D**)] Total lysates (C), soluble tubulin fractions and polymeric tubulin fractions (D) of NIH-3T3 cells stably expressing FLAG-HA-tagged UCH-L1 were analyzed by immunoblotting. (**E**) Interactions of proteins with microtubules. After the tubulin polymerization assay, the polymerized tubulin was pelleted by centrifugation. The indicated volumes of samples from the supernatants (S) and the pellets (P) were analyzed by CBB staining. BSA was used as a control that does not specifically interact with microtubules. The amount of BSA detected in the pellet fraction was approximately one-twelfth of the amount detected in the supernatant fraction. UCH-L1 levels in the pellet fraction were below detectable levels. (**F**) Differentiated Neuro2a cells transfected with the indicated constructs were incubated with or without 5 μM paclitaxel for 24 h. Cell death was assessed by a lactate dehydrogenase release assay. Data are expressed as the means ± SD ($n = 4$). $^{**}P < 0.01$ (t-test).

DISCUSSION

Our previous study using CD suggests that the I93M mutation increases the β-sheet content, but reduces the α-helix content of UCH-L1 (9). We have also shown, using small-angle neutron scattering, that UCH-L1^{WT} has an ellipsoidal shape, whereas UCH-L1^{I93M} has a more globular shape in an aqueous solution (10). However, the biochemical and molecular properties of UCH-L1^{I93M} in mammalian cells, as well as the molecular mechanisms that underlie UCH-L1^{I93M}-associated PD, have not been elucidated. In this study, we have shown that, compared with UCH-L1^{WT}, UCH-L1^{I93M} displays

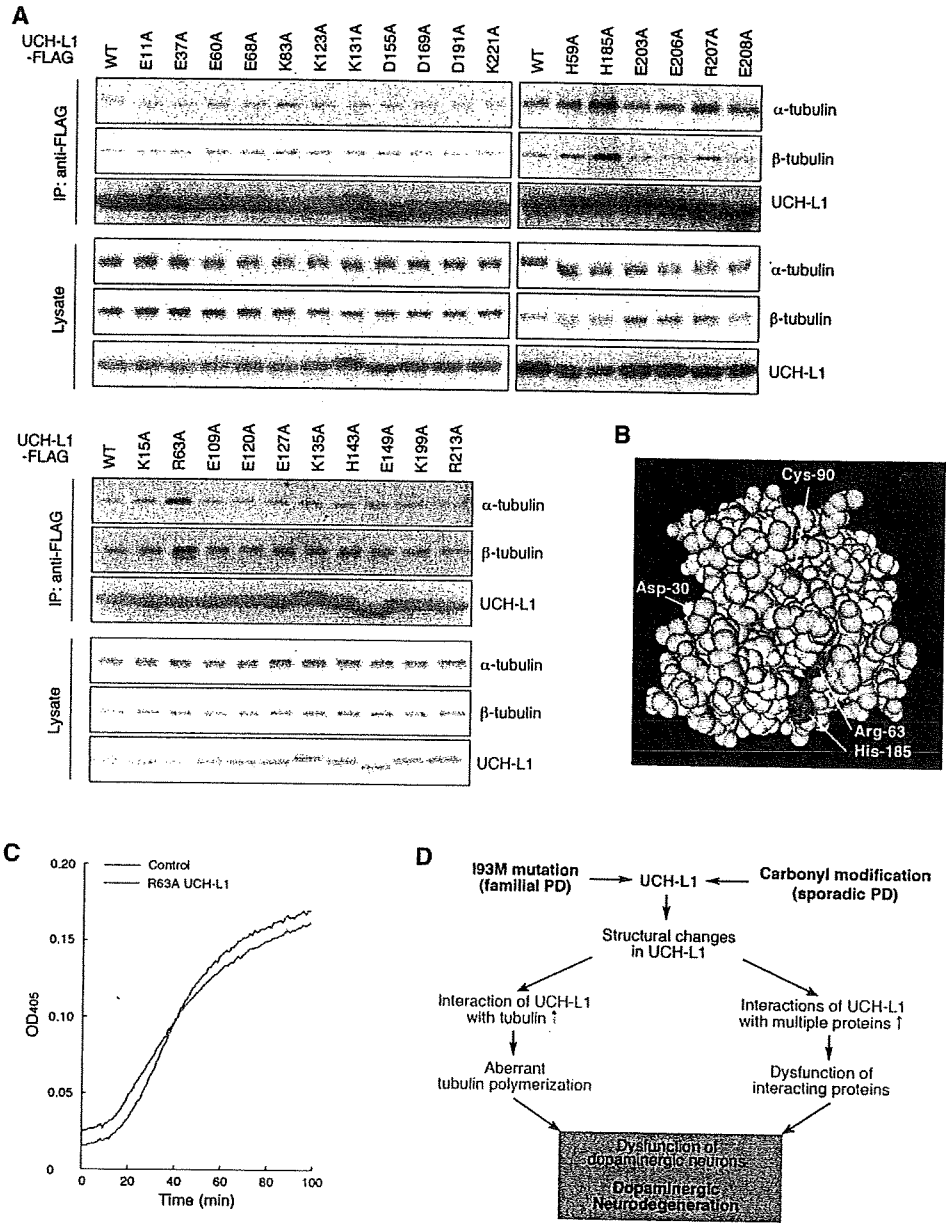

Figure 7. Amino acid residues of UCH-L1 involved in the interaction with tubulin. (**A**) Alanine-scanning mutagenesis of UCH-L1. Lysates of COS-7 cells transfected with the indicated constructs were immunoprecipitated with anti-FLAG antibody and analyzed by immunoblotting. (**B**) Structural model for human UCH-L1. Cys-90 is shown in blue, Arg-63 and His-185 are in magenta and basic and acidic amino acid residues that had no effect on tubulin interaction (Figs 5B and7A) are shown in white, using NCBI's structural model (mmdbId:38174). (**C**) A tubulin polymerization assay was performed in the absence (control) or in the presence of recombinant UCH-L1. (**D**) Schematic representation of a model for the roles of UCH-L1^{I93M} and carbonyl-modified UCH-L1 in PD. The I93M mutation (as occurs in familial PD associated with UCH-L1^{I93M}) and carbonyl modification (as occurs in sporadic PD) cause conformational changes in UCH-L1. Owing to the excess of oxidative stresses including HNE (in the case of sporadic PD) and the abundant expression of UCH-L1 in dopaminergic neurons, abnormal UCH-L1 proteins are overproduced in dopaminergic neurons. Abnormal UCH-L1 interacts with tubulin and aberrantly modulates tubulin polymerization. The aberrant interactions of UCH-L1 variants with multiple proteins may also cause dysfunctions of interacting proteins. The deregulations of abnormal UCH-L1-interacting proteins, including tubulin, result in dysfunction of dopaminergic neurons, leading to neurodegeneration.

increased insolubility, which is characteristic of several neurodegenerative disease-linked mutants, aberrantly elevated interactions with multiple proteins over 30 kDa and decreased interaction with monoubiquitin (Fig. 1). Taken together, our new and previous findings indicate that the I93M mutation in UCH-L1 alters its conformation, resulting in changes in the biochemical properties of UCH-L1.

Similar to UCH-L1^{I93M}, other dominantly inherited neurodegenerative disease-linked mutants, such as mutant SOD1 and mutant α-synuclein, cause neurodegeneration, presumably

via an acquired toxicity. Studies of the mutants strongly suggest that abnormally increased interactions of these mutant proteins with other proteins constitute a cause of disease (22–25). Therefore we screened for UCH-L1-interacting proteins using a coIP assay and subsequent LC-MS/MS analysis. We found that tubulin is a novel UCH-L1-interacting protein, and that the interactions of UCH-L1^{I93M} with these proteins are increased compared with those of UCH-L1^{WT} (Fig. 5B). We have also shown that UCH-L1^{I93M} promotes tubulin polymerization and stabilizes microtubules (Fig. 6B–D). UCH-L1^{I93M} and paclitaxel coordinately induced neuronal cell death (Fig. 6F). Together with the fact that tightly regulated tubulin polymerization is essential for neurons to function and remain viable, and that abnormal microtubule dynamics and tubulin polymerization are associated with several neurodegenerative diseases (37,38), our results strongly suggest that aberrant tubulin polymerization caused by mutant UCH-L1 at least partly constitutes a toxic function of mutant UCH-L1. Other than tubulin, mutant UCH-L1 interacts with multiple proteins (Figs 1F and 5A). These other interactors may also be involved in the mechanism of UCH-L1-mediated neurodegeneration (Fig. 7D). We have identified some of these interactors (T.K. and K.W., unpublished data), and these proteins are currently under investigation.

It is known that the majority of PD cases occur sporadically, and that oxidative/carbonyl stresses are elevated in PD brains (12,13). However, the molecular mechanisms underlying the causes of sporadic PD have remained largely unknown. Choi *et al.* (12) have shown that UCH-L1 is a major target of carbonyl damage associated with sporadic PD, implying that carbonyl-modified UCH-L1 is involved in the cause of sporadic PD. In the present study, we found that carbonyl-modified UCH-L1 and UCH-L1^{I93M} share molecular and functional properties. Importantly, both UCH-L1s display shared properties in all of the experiments we performed (Supplementary Material, Table S2). These results strongly suggest that carbonyl-modified UCH-L1 is also toxic to neurons and constitutes one of the causes of sporadic PD. Considering that UCH-L1 is abundant in the brain (5), and that UCH-L1 is a major target of carbonyl damage in PD brains (12), it is possible that carbonyl-modified UCH-L1 is the major cause of the disease.

It has been reported that UCH-L1 mRNA is expressed abundantly in dopaminergic neurons in the human brain (41). Abundant expression of UCH-L1 protein in dopaminergic neurons was also observed in mouse brains (Supplementary Material, Fig. S4 and S5). Dopaminergic neurons are particularly exposed to oxidative and carbonyl stresses because dopamine can auto-oxidize into toxic dopamine quinone, superoxide radicals and hydrogen peroxide (42). In addition, it has been reported that oxidative stresses in dopaminergic neurons in sporadic PD brains are higher than the stresses in control brains (30). Thus, in PD, UCH-L1^{I93M} or oxidative/carbonyl-modified UCH-L1 is possibly overproduced in dopaminergic neurons, leading to the selective loss of dopaminergic neurons (Fig. 7D).

Oxidatively modified UCH-L1 has also been found in the brains of both familial and sporadic Alzheimer's disease (AD) patients (12,43,44). AD is characterized pathologically by deposition of the amyloid β-protein in the form of amyloid plaques in the brain, and the deposition of the amyloid β is thought to be a major cause of both familial and sporadic AD (20). Thus, although it is possible that toxicity of carbonyl-modified UCH-L1 is involved in amyloid β-mediated neurodegeneration in AD, carbonyl-modified UCH-L1 may not be the primary cause of AD. A recent report has shown that brains from patients with sporadic PD and AD contain decreased levels of UCH-L1 (30 and 50% decrease, respectively) (12). Gong *et al.* (45) showed that the introduction of exogenous UCH-L1 rescued the synaptic and cognitive functions of AD model mice, which exhibit decreased levels of UCH-L1 in their hippocampi. We have also shown that mice deficient in UCH-L1 exhibit memory dysfunction (46). These findings indicate that a reduction in the levels of functional UCH-L1 may contribute to the pathogenesis of AD. Oxidative modification of several proteins, including antioxidant proteins, is found in mice deficient in UCH-L1 (47), suggesting involvement of these proteins in AD. Since diminution of the proteasome activity may lead to neurodegeneration (48), it is also possible that decreased UCH-L1 function leads to dysfunction of the ubiquitin-proteasome system and this dysfunction contributes to neurodegeneration in AD. On the contrary, mice deficient in UCH-L1 do not exhibit obvious dopaminergic cell loss, indicating that a loss or decrease in the level of UCH-L1 is not the main cause of PD. Investigation of the relationship between the specificity of brain areas that is affected by oxidative stress and genetic or environmental factors should generate further insights into the mechanism of oxidative stress in the pathogenesis of sporadic PD and AD.

In conclusion, familial PD-associated UCH-L1^{I93M} and carbonyl-modified UCH-L1, which is associated with sporadic PD, display common aberrant properties. Thus, UCH-L1^{I93M} would be a useful tool for studying the molecular mechanism underlying sporadic PD. We propose that the abnormal interactions of UCH-L1 variants with other proteins including tubulin constitute one of the causes of not only familial PD associated with UCH-L1^{I93M}, but also sporadic PD, and can be therapeutic targets for these diseases and possibly for other neurodegenerative diseases.

MATERIALS AND METHODS

Plasmids

pCI-neo-hUCH-L1 plasmids containing human WT UCH-L1 and UCH-L1 variants with or without FLAG tag were prepared as described previously (49) or generated using a QuikChange Site-Directed Mutagenesis Kit (Stratagene, La Jolla, CA, USA). The expression plasmid pCR3-hα-synuclein containing FLAG-tagged human α-synuclein was kindly donated by Ryosuke Takahashi (Kyoto University, Kyoto, Japan) and Yuzuru Imai (Tohoku University, Miyagi, Japan) (50). The pcDNA3-hSOD1 expression plasmids containing WT, A4V, G85R or G93A mutant SOD1, and pCI-hα-synuclein expression plasmids containing WT, A30P or A53T mutant α-synuclein were prepared as described previously (17). The expression plasmid pEF-hUCH-L1 containing WT UCH-L1 was constructed by ligating the cDNA

encoding UCH-L1 into pEF-BOS vector (51). The bacterial expression plasmid pPROTetE-hUCH-L1 containing 6HN-tagged UCH-L1 was prepared as described previously (9). pGEX-hUCH-L1 bacterial expression plasmids containing WT, I93M or R63A UCH-L1 with a GST-tag were constructed by ligating the cDNA encoding each UCH-L1 into pGEX-6P-1 vector (GE Healthcare UK Ltd, Buckinghamshire HP7 9NA, UK).

Cell culture and transfection

Neuro2a, SH-SY5Y, COS-7 and HeLa cells were maintained in Dulbecco's modified Eagle's medium (Sigma, St Louis, MO, USA) supplemented with 10% fetal bovine serum (JRH Biosciences, Lenexa, KS, USA). NIH-3T3 cells stably expressing human UCH-L1 with a FLAG-HA double-tag at the N terminus were cultured as described previously (49). Transient transfection of Neuro2a, SH-SY5Y and COS-7 cells with each vector was performed using the FuGENE 6 Transfection Reagent (Roche Diagnostics, Indianapolis, IN, USA), TransFectin Lipid Reagent (Bio-Rad, Hercules, CA, USA) and Lipofectamine Reagent (Invitrogen, Carlsbad, CA, USA), respectively. For the experiments investigating the carbonyl modification of UCH-L1, cells were incubated at 37°C for 90 min with each carbonyl compound or H_2O_2 in PBS containing 5 mM glucose, 0.3 mM $CaCl_2$ and 0.62 mM $MgCl_2$.

Immunoblotting

SDS–PAGE was performed under reducing conditions. Immunoblotting was performed according to standard procedures. The preparation of detergent (1% Triton X-100)-soluble and -insoluble fractions was performed as described previously (17). Mouse anti-α-tubulin and anti-β-tubulin antibodies were purchased from Sigma. Rabbit anti-α-tubulin and anti-β-tubulin antibodies were from Cell Signaling (Danvers, MA, USA). Mouse anti-HNE and rabbit anti-HNE antibodies were from Oxis (Portland, OR, USA) and Alpha Diagnostic (San Antonio, TX, USA), respectively. Antibodies against SOD1, UCH-L1 and reduced-HNE were purchased from Stressgen Bioreagents (Victoria, BC, Canada), UltraClone (England, UK) and Calbiochem (Darmstadt, Germany), respectively. Anti-β-actin, ubiquitin and FLAG antibodies were from Sigma. The antibody against α-synuclein was from Chemicon (Temecula, CA, USA). For immunoblotting with anti-reduced HNE antibody, the proteins on a PVDF membrane were reduced with 10 mM $NaBH_4$ in Tris-buffered saline for 30 min at room temperature before being reacted with anti-reduced HNE antibody. Carbonyl modification of proteins was detected using an OxyBlot Protein Oxidation Detection Kit (Chemicon) containing an anti-DNP antibody.

Immunoprecipitation

Immunoprecipitation was performed as previously described (52). Cells were harvested by cold immunoprecipitation buffer (15 mM Tris pH 7.5, 120 mM NaCl, 25 mM KCl, 2 mM EGTA, 2 mM EDTA, 0.5% Triton X-100 and protease inhibitors). The lysates were centrifuged at 20 000*g* for 10 min at 4°C. The supernatant was subjected to immunoprecipitation. Lysates (1 mg protein in immunoprecipitation buffer) were incubated with 5 μg of antibody for 12 h. Twenty microliters of protein G Sepharose (GE Healthcare) was then added, and incubation was continued for 1 h. For the immunoprecipitation of FLAG-tagged proteins, lysates (1–2 mg protein in immunoprecipitation buffer) were incubated with 30 μl anti-FLAG M2 affinity gel (Sigma) for 2 h. After the beads were washed three times with immunoprecipitation buffer, proteins were eluted with SDS sample buffer (10 mM Tris, pH 7.8, 3% SDS, 5% glycerol and 0.02% bromophenol blue). In some experiments, proteins were eluted with SDS sample buffer containing 2% 2-mercaptoethanol. For the immunoprecipitation of endogenous UCH-L1 (Fig. 5D), 100 μg anti-UCH-L1 antibody (53) or 100 μg normal rabbit IgG (Santa Cruz Biotechnology, Santa Cruz, CA, USA) was immobilized to 100 μl of protein G beads using a Seize X Protein G Immnoprecipitation Kit (Pierce, Rockford, IL, USA). Cell lysates (1 mg protein in 50 mM Tris, pH 7.5, 150 mM NaCl, 5 mM EDTA, 0.25% Triton X-100 and protease inhibitors) were incubated with 25 μl of beads for 12 h. Protein G beads without antibody and protein G beads cross-linked with normal rabbit IgG were used as controls.

Mass spectrometry analysis

Protein bands were sliced from the gel and subjected to in-gel trypsin digestion, and LC-MS/MS analysis was performed at APRO Life Science Institute, Inc. (Naruto, Japan) as a custom service.

Circular dichroism

CD measurements of 0.1 mg/ml (4 μM) of recombinant human UCH-L1 without a tag (Boston Biochem, Cambridge, MA, USA) in 20 mM sodium phosphate buffer (pH 8.0) were performed as described previously (9,10). Since two cysteine residues in UCH-L1, Cys-90 and Cys-152, are major targets of HNE modification (Fig. 4), 4 μM UCH-L1 was reacted with 8 μM HNE. Far UV CD spectra (190–250 nm) were recorded in a 1 mm quartz cuvette on a Jasco J-820 spectropolarimeter (Jasco, Tokyo, Japan) equipped with a temperature controller by scanning at a rate of 50 nm/min at 25°C. For all spectra, 12 scans were averaged. All CD spectra were corrected by background subtraction of the spectrum obtained with buffer alone and smoothed. Spectra were analyzed for the percentage of secondary structural elements by a computer program, based on an algorithm that compares experimental spectra with those of known proteins (54).

Preparation of recombinant proteins

6HN-tagged human UCH-L1 proteins were prepared as described previously (9). For purification of UCH-L1 without a tag, the pGEX UCH-L1 vectors were transformed into *Escherichia coli* BL21. Production of fusion proteins was induced by the addition of isopropyl-β-D-thiogalactopyranoside to a final concentration of 0.5 mM. After a 4 h induction at 37°C, the cells were harvested and lysed by sonication in PBS containing 1% Triton X-100 and protease inhibitors. Puri-

fication of GST-tagged UCH-L1 was performed using glutathione Sepharose 4B (GE Healthcare), and UCH-L1 was released from GST by digestion using PreScission Protease (GE Healthcare). Purified proteins were resolved by SDS–PAGE under reducing conditions and visualized by Coomassie brilliant blue R-250 to confirm purity (Supplementary Material, Fig. S6).

Pull-down assay

TALON resin (Clontech, Palo Alto, CA, USA) was blocked with 3% BSA for 1 h in order to prevent non-specific binding of tubulin (data not shown) and washed three times with PBS containing 0.05% Triton X-100. Five micrograms of recombinant UCH-L1 with an HN tag and 5 μg of purified tubulin (>99% pure tubulin, Cytoskeleton, Denver, CO, USA) were mixed and incubated for 4 h in PBS containing 0.05% Triton X-100. As a control, vehicle was mixed instead of UCH-L1. Twenty microliters of TALON resin blocked with BSA was then added, and incubation was continued for 1 h. After beads were washed three times with PBS containing 0.05% Triton X-100, proteins were eluted with SDS sample buffer.

Tubulin polymerization assay

An *in vitro* tubulin polymerization assay was performed using a tubulin polymerization assay kit, OD based, >99% pure tubulin (Cytoskeleton), according to the manufacturer's protocol. Briefly, recombinant UCH-L1 without a tag and tubulin were mixed to give a final concentration of 0.05 mg/ml UCH-L1 and 3 mg/ml tubulin in tubulin polymerization buffer (80 mM PIPES, pH 6.9, 2 mM $MgCl_2$, 0.5 mM EGTA, 1 mM GTP, 5% glycerol) and subjected to a tubulin polymerization assay. As a control, vehicle was mixed instead of UCH-L1. Since two cysteine residues in UCH-L1 are major targets of HNE modification (Fig. 4), 40 μM UCH-L1 was reacted with 80 μM HNE to prepare the HNE-modified UCH-L1. To analyze the interaction between UCH-L1 and polymerized tubulin, the polymerized tubulin was pelleted by centrifugation after a tubulin polymerization assay. The supernatant (100 μl) was mixed with 50 μl of 3× SDS sample buffer (30 mM Tris, pH 7.8, 9% SDS, 15% glycerol, 0.06% bromophenol blue). The pellet was washed twice with tubulin polymerization buffer and then dissolved in 150 μl of SDS sample buffer.

Preparation of cell extracts containing soluble and polymeric tubulin

Preparation of soluble and polymeric fractions of tubulin was performed as described (55) with slight modification. Briefly, cells were washed very gently with a microtubule stabilizing buffer (0.1 M *N*-morpholinoethanesulfonic acid, pH 6.75, 1 mM $MgSO_4$, 2 mM EGTA, 0.1 mM EDTA, 4 M glycerol). Soluble proteins were extracted at 37°C for 5 min in microtubule stabilizing buffer containing 0.04% saponin. The remaining cytoskeletal fraction in the culture dish was washed with microtubule stabilizing buffer containing 0.4% saponin and dissolved in SDS sample buffer.

Quantitative assessment of cell death

Neuro2a cells were transfected with plasmids. Four hours after transfection, neuronal cell differentiation was induced by addition of 5 mM dibutyryl cAMP as described in the literature (40), and cells were incubated for 24 h. Cells were then incubated with or without 5 μM paclitaxel for another 24 h. Cell death was assessed by a lactate dehydrogenase release assay, as described previously (17).

Statistical analysis

For comparison of two groups, the statistical difference was determined by Student's *t*-test.

SUPPLEMENTARY MATERIAL

Supplementary Material is available at HMG Online.

ACKNOWLEDGEMENTS

We thank Dr Ryosuke Takahashi (Kyoto University) and Dr Yuzuru Imai (Tohoku University) for the gift of pCR3-hα-synuclein plasmid, Dr Yasuyuki Suzuki (National Institute of Neuroscience) for valuable discussion; Naoki Takagaki (National Institute of Neuroscience) for support with English.

Conflict of Interest statement. None declared.

FUNDING

This work was supported by Grants-in-Aid for Scientific Research of Japan Society for the Promotion of Science; Research Grant in Priority Area Research of the Ministry of Education, Culture, Sports, Science and Technology, Japan; Grants-in-Aid for Scientific Research of the Ministry of Health, Labour and Welfare, Japan; Program for Promotion of Fundamental Studies in Health Sciences of the National Institute of Biomedical Innovation (NIBIO), Japan; New Energy and Industrial Technology Development Organization (NEDO), Japan.

REFERENCES

1. Leroy, E., Boyer, R., Auburger, G., Leube, B., Ulm, G., Mezey, E., Harta, G., Brownstein, M.J., Jonnalagada, S., Chernova, T. *et al.* (1998) The ubiquitin pathway in Parkinson's disease. *Nature*, **395**, 451–452.
2. Setsuie, R., Wang, Y.L., Mochizuki, H., Osaka, H., Hayakawa, H., Ichihara, N., Li, H., Furuta, A., Sano, Y., Sun, Y.J. *et al.* (2007) Dopaminergic neuronal loss in transgenic mice expressing the Parkinson's disease-associated UCH-L1 I93M mutant. *Neurochem. Int.*, **50**, 119–129.
3. Maraganore, D.M., Lesnick, T.G., Elbaz, A., Chartier-Harlin, M.C., Gasser, T., Kruger, R., Hattori, N., Mellick, G.D., Quattrone, A., Satoh, J. *et al.* (2004) UCHL1 is a Parkinson's disease susceptibility gene. *Ann. Neurol.*, **55**, 512–521.
4. Healy, D.G., Abou-Sleiman, P.M., Casas, J.P., Ahmadi, K.R., Lynch, T., Gandhi, S., Muqit, M.M., Foltynie, T., Barker, R., Bhatia, K.P. *et al.* (2006) UCHL-1 is not a Parkinson's disease susceptibility gene. *Ann. Neurol.*, **59**, 627–633.
5. Wilkinson, K.D., Lee, K.M., Deshpande, S., Duerksen-Hughes, P., Boss, J.M. and Pohl, J. (1989) The neuron-specific protein PGP 9.5 is a ubiquitin carboxyl-terminal hydrolase. *Science*, **246**, 670–673.

6. Larsen, C.N., Krantz, B.A. and Wilkinson, K.D. (1998) Substrate specificity of deubiquitinating enzymes: ubiquitin C-terminal hydrolases. *Biochemistry*, **37**, 3358–3368.
7. Liu, Y., Fallon, L., Lashuel, H.A., Liu, Z. and Lansbury, P.T., Jr (2002) The UCH-L1 gene encodes two opposing enzymatic activities that affect alpha-synuclein degradation and Parkinson's disease susceptibility. *Cell*, **111**, 209–218.
8. Osaka, H., Wang, Y.L., Takada, K., Takizawa, S., Setsuie, R., Li, H., Sato, Y., Nishikawa, K., Sun, Y.J., Sakurai, M. *et al.* (2003) Ubiquitin carboxy-terminal hydrolase L1 binds to and stabilizes monoubiquitin in neuron. *Hum. Mol. Genet.*, **12**, 1945–1958.
9. Nishikawa, K., Li, H., Kawamura, R., Osaka, H., Wang, Y.L., Hara, Y., Hirokawa, T., Manago, Y., Amano, T., Noda, M. *et al.* (2003) Alterations of structure and hydrolase activity of parkinsonism-associated human ubiquitin carboxyl-terminal hydrolase L1 variants. *Biochem. Biophys. Res. Commun.*, **304**, 176–183.
10. Naito, S., Mochizuki, H., Yasuda, T., Mizuno, Y., Furusaka, M., Ikeda, S., Adachi, T., Shimizu, H.M., Suzuki, J., Fujiwara, S. *et al.* (2006) Characterization of multimetric variants of ubiquitin carboxyl-terminal hydrolase L1 in water by small-angle neutron scattering. *Biochem. Biophys. Res. Commun.*, **339**, 717–725.
11. Saigoh, K., Wang, Y.L., Suh, J.G., Yamanishi, T., Sakai, Y., Kiyosawa, H., Harada, T., Ichihara, N., Wakana, S., Kikuchi, T. *et al.* (1999) Intragenic deletion in the gene encoding ubiquitin carboxy-terminal hydrolase in gad mice. *Nat. Genet.*, **23**, 47–51.
12. Choi, J., Levey, A.I., Weintraub, S.T., Rees, H.D., Gearing, M., Chin, L.S. and Li, L. (2004) Oxidative modifications and down-regulation of ubiquitin carboxyl-terminal hydrolase L1 associated with idiopathic Parkinson's and Alzheimer's diseases. *J. Biol. Chem.*, **279**, 13256–13264.
13. Ischiropoulos, H. and Beckman, J.S. (2003) Oxidative stress and nitration in neurodegeneration: cause, effect, or association? *J. Clin. Invest.*, **111**, 163–169.
14. Lowe, J., McDermott, H., Landon, M., Mayer, R.J. and Wilkinson, K.D. (1990) Ubiquitin carboxyl-terminal hydrolase (PGP 9.5) is selectively present in ubiquitinated inclusion bodies characteristic of human neurodegenerative diseases. *J. Pathol.*, **161**, 153–160.
15. Lee, M.K., Stirling, W., Xu, Y., Xu, X., Qui, D., Mandir, A.S., Dawson, T.M., Copeland, N.G., Jenkins, N.A. and Price, D.L. (2002) Human alpha-synuclein-harboring familial Parkinson's disease-linked Ala-53→Thr mutation causes neurodegenerative disease with alpha-synuclein aggregation in transgenic mice. *Proc. Natl Acad. Sci. USA*, **99**, 8968–8973.
16. Johnston, J.A., Dalton, M.J., Gurney, M.E. and Kopito, R.R. (2000) Formation of high molecular weight complexes of mutant Cu,Zn-superoxide dismutase in a mouse model for familial amyotrophic lateral sclerosis. *Proc. Natl Acad. Sci. USA*, **97**, 12571–12576.
17. Kabuta, T., Suzuki, Y. and Wada, K. (2006) Degradation of amyotrophic lateral sclerosis-linked mutant Cu,Zn-superoxide dismutase proteins by macroautophagy and the proteasome. *J. Biol. Chem.*, **281**, 30524–30533.
18. Lewis, J., McGowan, E., Rockwood, J., Melrose, H., Nacharaju, P., Van Slegtenhorst, M., Gwinn-Hardy, K., Paul Murphy, M., Baker, M., Yu, X. *et al.* (2000) Neurofibrillary tangles, amyotrophy and progressive motor disturbance in mice expressing mutant (P301L) tau protein. *Nat. Genet.*, **25**, 402–405.
19. Ardley, H.C., Scott, G.B., Rose, S.A., Tan, N.G. and Robinson, P.A. (2004) UCH-L1 aggresome formation in response to proteasome impairment indicates a role in inclusion formation in Parkinson's disease. *J. Neurochem.*, **90**, 379–391.
20. Haass, C. and Selkoe, D.J. (2007) Soluble protein oligomers in neurodegeneration: lessons from the Alzheimer's amyloid beta-peptide. *Nat. Rev. Mol. Cell Biol.*, **8**, 101–112.
21. Arrasate, M., Mitra, S., Schweitzer, E.S., Segal, M.R. and Finkbeiner, S. (2004) Inclusion body formation reduces levels of mutant huntingtin and the risk of neuronal death. *Nature*, **431**, 805–810.
22. Pasinelli, P., Belford, M.E., Lennon, N., Bacskai, B.J., Hyman, B.T., Trotti, D. and Brown, R.H., Jr (2004) Amyotrophic lateral sclerosis-associated SOD1 mutant proteins bind and aggregate with Bcl-2 in spinal cord mitochondria. *Neuron*, **43**, 19–30.
23. Zhang, F., Strom, A.L., Fukada, K., Lee, S., Hayward, L.J. and Zhu, H. (2007) Interaction between familial amyotrophic lateral sclerosis (ALS)-linked SOD1 mutants and the dynein complex. *J. Biol. Chem.*, **282**, 16691–16699.
24. Urushitani, M., Sik, A., Sakurai, T., Nukina, N., Takahashi, R. and Julien, J.P. (2006) Chromogranin-mediated secretion of mutant superoxide dismutase proteins linked to amyotrophic lateral sclerosis. *Nat. Neurosci.*, **9**, 108–118.
25. Cuervo, A.M., Stefanis, L., Fredenburg, R., Lansbury, P.T. and Sulzer, D. (2004) Impaired degradation of mutant alpha-synuclein by chaperone-mediated autophagy. *Science*, **305**, 1292–1295.
26. Schaffar, G., Breuer, P., Boteva, R., Behrends, C., Tzvetkov, N., Strippel, N., Sakahira, H., Siegers, K., Hayer-Hartl, M. and Hartl, F.U. (2004) Cellular toxicity of polyglutamine expansion proteins: mechanism of transcription factor deactivation. *Mol. Cell*, **15**, 95–105.
27. Uchida, K. (2000) Role of reactive aldehyde in cardiovascular diseases. *Free Radic. Biol. Med.*, **28**, 1685–1696.
28. Uchida, K. (2003) Histidine and lysine as targets of oxidative modification. *Amino Acids*, **25**, 249–257.
29. Stadtman, E.R. (1993) Oxidation of free amino acids and amino acid residues in proteins by radiolysis and by metal-catalyzed reactions. *Annu. Rev. Biochem.*, **62**, 797–821.
30. Yoritaka, A., Hattori, N., Uchida, K., Tanaka, M., Stadtman, E.R. and Mizuno, Y. (1996) Immunohistochemical detection of 4-hydroxynonenal protein adducts in Parkinson disease. *Proc. Natl Acad. Sci. USA*, **93**, 2696–2701.
31. Castellani, R.J., Perry, G., Siedlak, S.L., Nunomura, A., Shimohama, S., Zhang, J., Montine, T., Sayre, L.M. and Smith, M.A. (2002) Hydroxynonenal adducts indicate a role for lipid peroxidation in neocortical and brainstem Lewy bodies in humans. *Neurosci. Lett.*, **319**, 25–28.
32. Das, C., Hoang, Q.Q., Kreinbring, C.A., Luchansky, S.J., Meray, R.K., Ray, S.S., Lansbury, P.T., Ringe, D. and Petsko, G.A. (2006) Structural basis for conformational plasticity of the Parkinson's disease-associated ubiquitin hydrolase UCH-L1. *Proc. Natl Acad. Sci. USA*, **103**, 4675–4680.
33. Tiwari, A., Xu, Z. and Hayward, L.J. (2005) Aberrantly increased hydrophobicity shared by mutants of Cu,Zn-superoxide dismutase in familial amyotrophic lateral sclerosis. *J. Biol. Chem.*, **280**, 29771–29779.
34. Richardson, J.S. and Richardson, D.C. (2002) Natural beta-sheet proteins use negative design to avoid edge-to-edge aggregation. *Proc. Natl Acad. Sci. USA*, **99**, 2754–2759.
35. Lee, J.J. and Swain, S.M. (2006) Peripheral neuropathy induced by microtubule-stabilizing agents. *J. Clin. Oncol.*, **24**, 1633–1642.
36. Figueroa-Masot, X.A., Hetman, M., Higgins, M.J., Kokot, N. and Xia, Z. (2001) Taxol induces apoptosis in cortical neurons by a mechanism independent of Bcl-2 phosphorylation. *J. Neurosci.*, **21**, 4657–4667.
37. Panda, D., Samuel, J.C., Massie, M., Feinstein, S.C. and Wilson, L. (2003) Differential regulation of microtubule dynamics by three- and four-repeat tau: implications for the onset of neurodegenerative disease. *Proc. Natl Acad. Sci. USA*, **100**, 9548–9553.
38. Fanara, P., Banerjee, J., Hueck, R.V., Harper, M.R., Awada, M., Turner, H., Husted, K.H., Brandt, R. and Hellerstein, M.K. (2007) Stabilization of hyperdynamic microtubules is neuroprotective in amyotrophic lateral sclerosis. *J. Biol. Chem.*, **282**, 23465–23472.
39. Tam, S., Geller, R., Spiess, C. and Frydman, J. (2006) The chaperonin TRiC controls polyglutamine aggregation and toxicity through subunit-specific interactions. *Nat. Cell Biol.*, **8**, 1155–1162.
40. Kitamura, A., Kubota, H., Pack, C.G., Matsumoto, G., Hirayama, S., Takahashi, Y., Kimura, H., Kinjo, M., Morimoto, R.I. and Nagata, K. (2006) Cytosolic chaperonin prevents polyglutamine toxicity with altering the aggregation state. *Nat. Cell Biol.*, **8**, 1163–1170.
41. Solano, S.M., Miller, D.W., Augood, S.J., Young, A.B. and Penney, J.B., Jr (2000) Expression of alpha-synuclein, parkin, and ubiquitin carboxy-terminal hydrolase L1 mRNA in human brain: genes associated with familial Parkinson's disease. *Ann. Neurol.*, **47**, 201–210.
42. Lotharius, J. and Brundin, P. (2002) Pathogenesis of Parkinson's disease: dopamine, vesicles and alpha-synuclein. *Nat. Rev. Neurosci.*, **3**, 932–942.
43. Castegna, A., Aksenov, M., Aksenova, M., Thongboonkerd, V., Klein, J.B., Pierce, W.M., Booze, R., Markesbery, W.R. and Butterfield, D.A. (2002) Proteomic identification of oxidatively modified proteins in Alzheimer's disease brain. Part I: creatine kinase BB, glutamine synthase, and ubiquitin carboxy-terminal hydrolase L-1. *Free Radic. Biol. Med.*, **33**, 562–571.
44. Butterfield, D.A., Gnjec, A., Poon, H.F., Castegna, A., Pierce, W.M., Klein, J.B. and Martins, R.N. (2006) Redox proteomics identification of

oxidatively modified brain proteins in inherited Alzheimer's disease: an initial assessment. *J. Alzheimers Dis.*, **10**, 391–397.
45. Gong, B., Cao, Z., Zheng, P., Vitolo, O.V., Liu, S., Staniszewski, A., Moolman, D., Zhang, H., Shelanski, M. and Arancio, O. (2006) Ubiquitin hydrolase Uch-L1 rescues beta-amyloid-induced decreases in synaptic function and contextual memory. *Cell*, **126**, 775–788.
46. Sakurai, M., Sekiguchi, M., Zushida, K., Yamada, K., Nagamine, S., Kabuta, T. and Wada, K. (2008) Reduction of memory in passive avoidance learning, exploratory behavior and synaptic plasticity in mice with a spontaneous deletion in the ubiquitin C-terminal hydrolase L1 gene. *Eur. J. Neurosci.*, **27**, 691–701.
47. Castegna, A., Thongboonkerd, V., Klein, J., Lynn, B.C., Wang, Y.L., Osaka, H., Wada, K. and Butterfield, D.A. (2004) Proteomic analysis of brain proteins in the gracile axonal dystrophy (gad) mouse, a syndrome that emanates from dysfunctional ubiquitin carboxyl-terminal hydrolase L-1, reveals oxidation of key proteins. *J. Neurochem.*, **88**, 1540–1546.
48. Halliwell, B. (2006) Proteasomal dysfunction: a common feature of neurodegenerative diseases? Implications for the environmental origins of neurodegeneration. *Antioxid. Redox Signal.*, **8**, 2007–2019.
49. Sakurai, M., Ayukawa, K., Setsuie, R., Nishikawa, K., Hara, Y., Ohashi, H., Nishimoto, M., Abe, T., Kudo, Y., Sekiguchi, M. *et al.* (2006) Ubiquitin C-terminal hydrolase L1 regulates the morphology of neural progenitor cells and modulates their differentiation. *J. Cell Sci.*, **119**, 162–171.
50. Imai, Y., Soda, M. and Takahashi, R. (2000) Parkin suppresses unfolded protein stress-induced cell death through its E3 ubiquitin-protein ligase activity. *J. Biol. Chem.*, **275**, 35661–35664.
51. Mizushima, S. and Nagata, S. (1990) pEF-BOS, a powerful mammalian expression vector. *Nucleic Acids Res.*, **18**, 5322.
52. Kabuta, T., Hakuno, F., Asano, T. and Takahashi, S. (2002) Insulin receptor substrate-3 functions as transcriptional activator in the nucleus. *J. Biol. Chem.*, **277**, 6846–6851.
53. Sano, Y., Furuta, A., Setsuie, R., Kikuchi, H., Wang, Y.L., Sakurai, M., Kwon, J., Noda, M. and Wada, K. (2006) Photoreceptor cell apoptosis in the retinal degeneration of Uchl3-deficient mice. *Am. J. Pathol.*, **169**, 132–141.
54. Yang, J.T., Wu, C.S. and Martinez, H.M. (1986) Calculation of protein conformation from circular dichroism. *Methods Enzymol.*, **130**, 208–269.
55. Joshi, H.C. and Cleveland, D.W. (1989) Differential utilization of beta-tubulin isotypes in differentiating neurites. *J. Cell Biol.*, **109**, 663–673.

THE JOURNAL OF BIOLOGICAL CHEMISTRY VOL. 283, NO. 35, pp. 23731–23738, August 29, 2008

Aberrant Interaction between Parkinson Disease-associated Mutant UCH-L1 and the Lysosomal Receptor for Chaperone-mediated Autophagy*[S]

Received for publication, March 10, 2008, and in revised form, June 12, 2008 Published, JBC Papers in Press, June 12, 2008, DOI 10.1074/jbc.M801918200

Tomohiro Kabuta[‡1], Akiko Furuta[‡], Shunsuke Aoki[‡2], Koh Furuta[§], and Keiji Wada[‡3]

From the [‡]Department of Degenerative Neurological Diseases, National Institute of Neuroscience, National Center of Neurology and Psychiatry, 4-1-1 Ogawahigashi, Kodaira, Tokyo 187-8502, Japan and the [§]Division of Clinical Laboratories, National Cancer Center Hospital, 5-1-1 Tsukiji, Chuo-ku, Tokyo 104-0045, Japan

Parkinson disease (PD) is the most common neurodegenerative movement disorder. An increase in the amount of α-synuclein protein could constitute a cause of PD. α-Synuclein is degraded at least partly by chaperone-mediated autophagy (CMA). The I93M mutation in ubiquitin C-terminal hydrolase L1 (UCH-L1) is associated with familial PD. However, the relationship between α-synuclein and UCH-L1 in the pathogenesis of PD has remained largely unclear. In this study, we found that UCH-L1 physically interacts with LAMP-2A, the lysosomal receptor for CMA, and Hsc70 and Hsp90, which can function as components of the CMA pathway. These interactions were abnormally enhanced by the I93M mutation and were independent of the monoubiquitin binding of UCH-L1. In a cell-free system, UCH-L1 directly interacted with the cytosolic region of LAMP-2A. Expression of I93M UCH-L1 in cells induced the CMA inhibition-associated increase in the amount of α-synuclein. Our findings may provide novel insights into the molecular links between α-synuclein and UCH-L1 and suggest that aberrant interaction of mutant UCH-L1 with CMA machinery, at least partly, underlies the pathogenesis of PD associated with I93M UCH-L1.

Parkinson disease (PD)[4] is the most common neurodegenerative movement disorder characterized by progressive degeneration confined mostly to dopaminergic neurons in the substantia nigra pars compacta. Although the majority of PD cases occur sporadically, nine genes have been reported to be associated with familial forms of PD. Several missense mutations in the α-synuclein gene are linked to dominantly inherited PD (1–3). Duplication and triplication of the α-synuclein gene were also shown to cause familial PD or parkinsonism (4–6), indicating that increases in the levels of α-synuclein could constitute a cause of PD. α-Synuclein is a major component of cytoplasmic inclusions called Lewy bodies in the brains of patients with sporadic PD (7, 8). These findings raised the idea that α-synuclein plays a central role in the pathogenesis of PD. Therefore, elucidating the molecular relationships between α-synuclein and other familial PD-associated proteins is important for understanding the mechanisms that underlie the pathology of PD.

A missense mutation in the ubiquitin C-terminal hydrolase L1 (UCH-L1) gene, leading to an I93M substitution at the protein level, has been reported in two affected siblings of a German family with dominantly inherited PD (9). In this family, four of seven family members were affected with PD. However, the family members, except the two siblings, were not genotyped. There was an unaffected presumed carrier of the I93M mutation in the family. Therefore, the link between the I93M mutation and the development of PD has been questioned (10, 11). To clarify the link between the mutation and PD, we have generated UCH-L1^{I93M} transgenic mice and reported that these mice exhibit progressive dopaminergic cell loss (12). In addition, we have shown that, compared with UCH-L1^{WT}, UCH-L1^{I93M} exhibits increased insolubility and levels of interactions with other proteins in mammalian cells, features that are characteristic of several neurodegenerative disease-linked mutants (13). These findings suggest that the I93M mutation in UCH-L1 contributes to the pathogenesis of PD. UCH-L1 has also been identified as a component of several inclusion bodies characteristic of neurodegenerative diseases including Lewy bodies (14). A polymorphism in the UCH-L1 gene, resulting in an S18Y substitution at the amino acid residue level, has been reported to be associated with decreased risk of PD in certain populations but not in other populations (15, 16). We have also reported that UCH-L1^{I93M} and carbonyl-modified UCH-L1, which is associated with sporadic PD (17), display shared aberrant properties (13), suggesting that carbonyl-modified UCH-L1 constitutes one of the causes of sporadic PD.

* This work was supported by grants-in-aid for scientific research from the Japan Society for the Promotion of Science; a research grant in priority area research from the Ministry of Education, Culture, Sports, Science, and Technology, Japan; grants-in-aid for scientific research from the Ministry of Health, Labor, and Welfare, Japan; and the Program for Promotion of Fundamental Studies in Health Sciences of the National Institute of Biomedical Innovation and the New Energy and Industrial Technology Development Organization, Japan. The costs of publication of this article were defrayed in part by the payment of page charges. This article must therefore be hereby marked "*advertisement*" in accordance with 18 U.S.C. Section 1734 solely to indicate this fact.

[S] The on-line version of this article (available at http://www.jbc.org) contains supplemental "Experimental Procedures," Figs. S1 and S2, and an additional reference.

[1] To whom correspondence may be addressed. Tel.: 81-42-346-1715; Fax: 81-42-346-1745; E-mail: kabuta@ncnp.go.jp.

[2] Present address: Dept. of Bioscience and Bioinformatics, Kyushu Inst. of Technology, 680-4 Kawazu, Iizuka-shi, Fukuoka 820-8502, Japan.

[3] To whom correspondence may be addressed. Tel.: 81-42-346-1715; Fax: 81-42-346-1745; E-mail: wada@ncnp.go.jp.

[4] The abbreviations used are: PD, Parkinson disease; UCH-L1, ubiquitin C-terminal hydrolase L1; WT, wild-type; CMA, chaperone-mediated autophagy; LAMP-2, lysosome-associated membrane protein type 2; Hsc70, heat shock cognate protein 70; Hsp90, heat shock protein 90; GAPDH, glyceraldehyde-3-phosphate dehydrogenase.

UCH-L1 is one of the most abundant proteins in the brain (1–5% of total soluble protein) (18) and is thought to hydrolyze ubiquitin conjugates into monoubiquitin (19). UCH-L1 was also reported to function as a ubiquitin ligase for monoubiquitinated α-synuclein in a cell-free system (20). Other than these enzymatic activities, we have reported that UCH-L1 stabilizes monoubiquitin by binding to monoubiquitin in neurons (21). Although the hydrolase activity of UCH-L1^{I93M} and the binding of UCH-L1^{I93M} to monoubiquitin are decreased compared with those of UCH-L1^{WT} (9, 13, 22), we have shown that mice deficient in UCH-L1 do not display obvious dopaminergic cell loss (21, 23). These observations indicate that the main cause of UCH-L1^{I93M}-associated PD may not be a loss of UCH-L1 function but an acquired toxicity of UCH-L1^{I93M}. Our previous studies also suggest that aberrantly enhanced physical interactions between UCH-L1^{I93M} and multiple proteins, including tubulin, underlie the toxic functions of UCH-L1^{I93M} (13).

However, the molecular relationship between α-synuclein and UCH-L1 in the pathogenesis of PD has remained largely unclear. α-Synuclein is known to be degraded at least partly by chaperone-mediated autophagy (CMA) (24), in which substrate proteins are selectively transported to and degraded in lysosomes (25). In this study, we sought to identify novel UCH-L1-interacting proteins. We found that UCH-L1 physically interacts with lysosome-associated membrane protein type 2A (LAMP-2A), heat shock cognate protein 70 (Hsc70), and heat shock protein 90 (Hsp90), all of which are components of the CMA pathway (26). These interactions were enhanced by the I93M mutation in UCH-L1 and were independent of the interaction between monoubiquitin and UCH-L1. We also provide the data suggesting that the aberrant interaction of UCH-L1 with CMA machinery results in the accumulation of α-synuclein.

EXPERIMENTAL PROCEDURES

Plasmids—pCI-neo-hUCH-L1 plasmids containing human WT UCH-L1 and UCH-L1 variants with or without a FLAG tag were prepared as described previously (13). The regulatory expression plasmids pTRE-Tight-hUCH-L1 containing WT and I93M UCH-L1 with a FLAG tag at the C terminus of UCH-L1 were constructed by ligating the cDNA encoding UCH-L1 into the pTRE-Tight (Clontech) vector. The expression plasmid pCI-neo-hα-synuclein was constructed using the pCI-neo mammalian expression vector (Promega), and the expression plasmid pCI-neo-ΔDQ α-synuclein was generated using a QuikChange site-directed mutagenesis kit (Stratagene).

Cell Culture and Transfection—COS-7 cells were maintained in Dulbecco's modified Eagle's medium (Sigma) supplemented with 10% fetal bovine serum (JRH Biosciences, Lenexa, KS). IMR-90 cells, which have been used to study CMA (27), were cultured as described in the literature (27). NIH-3T3 cells stably expressing human UCH-L1 with a FLAG-hemagglutinin double tag at the N terminus were cultured as described previously (13). Transient transfection of COS-7 and IMR-90 cells with each vector was performed using Lipofectamine reagent (Invitrogen) and Lipofectamine LTX reagent (Invitrogen), respectively. There was no notable difference in the transfection efficiency among the culture dishes (wells) in our experimental conditions (data not shown).

Immunoblotting and Immunoprecipitation—Preparation of the detergent (1% Triton X-100)-soluble fraction was performed as described previously (28). The cytosolic fraction that does not contain LAMP-2, a marker of lysosomes, and the crude lysosomal fraction containing LAMP-2 (supplemental Fig. S1*A*) were prepared according to the method described by Pertoft *et al.* (29). SDS-PAGE was performed under reducing conditions. Immunoblotting was performed according to standard procedures as described previously (30). For some experiments, Can Get Signal Immunoreaction Enhancer Solution (Toyobo, Osaka, Japan) was used. The signal intensity was quantified by densitometry using FluorChem software (Alpha Innotech, San Leandro, CA). Immunoprecipitation was performed using anti-FLAG M2 affinity gel (Sigma) or 10 μg/ml antibodies (unless otherwise mentioned) with protein G-Sepharose (GE Healthcare), as described previously (13). The antibodies used were as follows. Antibodies against UCH-L1, Cu,Zn-superoxide dismutase 1, Hsc70, and Hsp90 were purchased from Ultra-Clone, Stressgen Bioreagents (Victoria, Canada), Affinity BioReagents (Golden, CO), and BD Transduction Laboratories (Franklin Lakes, NJ), respectively. Anti-β-actin, Mcl-1, and FLAG antibodies were from Sigma. Antibodies against α-synuclein and glyceraldehyde-3-phosphate dehydrogenase (GAPDH) were from Chemicon (Temecula, CA). Anti-p53 and Bcl-xL antibodies were from Cell Signaling. Anti-Bcl-2, Ubc9, NF-κB p65, and LAMP-2 antibodies were from Santa Cruz Biotechnology. The rabbit polyclonal anti-LAMP-2A antibody was raised in rabbit against a synthetic peptide (CYFIGLKHHHAGYEQF) containing an amino acid sequence corresponding to the cytosolic region of human LAMP-2A. The specificity of the anti-LAMP-2A antibody was confirmed as shown in supplemental Fig. S1, *B* and *C*.

Pulldown Assay—Recombinant human UCH-L1 proteins without a tag were prepared as described previously (13). A pulldown assay was performed as described previously (13) with slight modifications. Streptavidin-Sepharose (GE Healthcare) was blocked with 3% bovine serum albumin for 15 h to prevent nonspecific binding of UCH-L1 to the beads and washed three times with phosphate-buffered saline containing 0.05% Triton X-100. Ten μg of UCH-L1 (wild-type or I93M) and 2 nmol of synthetic peptides conjugated to biotin (control or LAMP-2A peptide, Invitrogen) were mixed and incubated for 15 h in phosphate-buffered saline containing 0.05% Triton X-100. Twenty μl of streptavidin beads blocked with bovine serum albumin was then added, and incubation was continued for 1 h. After beads were washed three times with phosphate-buffered saline containing 0.05% Triton X-100, proteins were eluted with SDS sample buffer and subjected to SDS-PAGE.

UCH-L1 Degradation Assay—COS-7 cells were cotransfected with pTet-Off and pTRE-Tight-hUCH-L1. Twenty-four h after transfection, transcription of UCH-L1-FLAG gene was suppressed by adding 100 ng/ml doxycycline and incubating for 4 h. Then, cells were harvested at the 0-, 24-, and 48-h time